

NASA CONTRACTOR  
REPORT



(NASA 12-29) 075

150

CODE-1

FACILITY FORM 602

N64-17831	
(ACCESSION NUMBER)	(THRU)
49	1
(PAGES)	(CODE)
	12
(NASA CR OR TNX OR AD NUMBER)	(CATEGORY)

THE MEASUREMENT OF UPPER-AIR  
DENSITY AND TEMPERATURE BY  
TWO RADAR-TRACKED  
FALLING SPHERES

by J. R. Patterson and K. D. McWalters (Michigan U.)  
Apr. 1964 42 p. mimeo

Prepared under Contract No. NASw-138 by  
UNIVERSITY OF MICHIGAN  
Ann Arbor, Michigan  
for

1037451

Double code

THE MEASUREMENT OF UPPER-AIR DENSITY AND TEMPERATURE  
BY TWO RADAR-TRACKED FALLING SPHERES

By J. W. Peterson and K. D. McWatters

*C NASA*  
Prepared under Contract No. NASw-138) by

UNIVERSITY OF MICHIGAN

Ann Arbor, Michigan

This report was reproduced photographically  
from copy supplied by the contractor.

NATIONAL AERONAUTICS AND SPACE ADMINISTRATION

---

For sale by the Office of Technical Services, Department of Commerce,  
Washington, D. C. 20230 -- Price \$1.50

## TABLE OF CONTENTS

	Page
LIST OF TABLES	v
LIST OF FIGURES	vii
LIST OF SYMBOLS	ix
THE UNIVERSITY OF MICHIGAN PROJECT PERSONNEL	xi
INTRODUCTION	1
I. DETAILS OF ROCKET FLIGHTS	2
II. DATA ANALYSIS PROCEDURES	4
III. DISCUSSION OF THE PROCESSED DATA	9
IV. ACKNOWLEDGMENTS	10
APPENDIX A. SOURCES OF $C_D$ DATA	11
APPENDIX B. CHOICE OF SMOOTHING PARAMETERS	13
APPENDIX C. EFFECTS OF WINDS	15
REFERENCES	18

## LIST OF TABLES

Table	Page
I. Nike-Cajun Rocket Flights, Wallops Island, Va.	19
II. Velocity Ratio vs. Altitude	20
III. Processed Data, Flight 10.50, 1-m Sphere	21
IV. Processed Data, Flight 10.43, 1-m Sphere	22
V. Processed Data, Flight 10.50, 7-in. Sphere, Up-leg Trajectory	23
VI. Processed Data, Flight 10.50, 7-in. Sphere, Down-leg Trajectory	24
VII. Drag Coefficient Function	25

PRECEDING PAGE BLANK NOT FILMED.

# LIST OF FIGURES

Figure	Page
1. Ejector pods on tail of Cajun.	26
2. Grenade Cajun nose cone, uncovered.	26
3. One-meter corner reflector sphere.	26
4. Altitude vs. distance down range.	27
5. Horizontal trajectory coordinates.	28
6. Altitude vs. time.	29
7. Velocity vs. altitude.	30
8. Density profiles, Flights 10.50 and 10.43.	31
9. FPS-16 radar AGC voltage.	32
10. Temperature profiles, Flights 10.50 and 10.43.	33
11. Mach Number vs. Reynolds Number of falling spheres.	34
12. JPL drag coefficient data.	35
13. $\bar{p}/\rho_0$ vs. $L/H$ .	36
14. Velocity vs. smoothing parameter $\Delta z_v$ .	37
15. Velocity components vs. smoothing parameter $\Delta z_v$ , 80 km.	38
16. Velocity components vs. smoothing parameter $\Delta z_v$ , 105 km.	39
17. Density function vs. smoothing parameter $\Delta z_v$ , 80 km.	40
18. Density function vs. smoothing parameter $\Delta z_v$ , 105 km.	41

PRECEDING PAGE BLANK NOT FILMED.

## LIST OF SYMBOLS

A	sphere cross section area
c	speed of sound
$C_D$	sphere drag coefficient
D	drag force
E	energy
g	gravity acceleration at altitude
$g_0$	gravity acceleration at altitude zero
H	scale height in the atmosphere
KE	kinetic energy per unit mass of sphere
m	mass of sphere
M	Mach Number
$M^*$	molecular weight of air
PE	potential energy per unit mass of sphere
$R^*$	universal gas constant
Re	Reynolds Number
r	radar coordinate slant range
$r_e$	radius of earth
s	distance along sphere trajectory
t	time
T	temperature, Kelvin
V	sphere velocity
$V_s$	sphere volume
$\alpha$	radar coordinate, azimuth angle
$\beta$	angle from line of sight to vertical
$\Delta$	difference
$\epsilon$	radar coordinate, elevation angle
$\rho$	density of air
$\mu$	viscosity of air

PRECEDING PAGE BLANK NOT FILMED.

THE UNIVERSITY OF MICHIGAN PROJECT PERSONNEL

Both Full- and Part-Time

Allen, Harold F., Ph.D., Research Engineer

Bodine, Margie S., Secretary

Bonfanti, Giovanni, B.S.(Ae.E.), Assistant in Research

Chapelsky, Orest, B.S.(Ae.E.), Assistant Research Engineer

Fischbach, Frederick F., M.S., Associate Research Mathematician

Hansen, William H., B.S., Research Engineer

Jones, Leslie M., B.S., Project Supervisor

McWatters, Kenneth D., B.S.E.(Aero.), Assistant Research Engineer

Mosakewicz, Mary C., Secretary

Peterson, John W., M.S., Research Engineer

Schaefer, Edward J., M.S., Research Engineer

PRECEDING PAGE BLANK NOT FILMED.

## INTRODUCTION

On NASA Contract No. NASw-138 the High Altitude Engineering Laboratory of The University of Michigan's Department of Aeronautical and Astronautical Engineering has been engaged in the development of rocket techniques and instruments for measuring the properties of the upper atmosphere. Two major lines of investigation have been pursued: the measurement of neutral composition with mass spectrometers, and the measurement of neutral density with falling spheres.

The purpose of the work described in this report was to develop an inexpensive technique for probing the atmosphere at relatively high levels using a lightweight sphere to be tracked by radar. It was anticipated that in order to satisfy the cost requirement, the sphere deployment system should be compatible with rocket payloads designed for other functions. Two such systems were developed and successfully flown on Nike-Cajun rockets.

The first system employed dual pods, which were arranged on the Cajun tail section for rearward deployment of two inflatable spheres. The nose cone payload of this rocket contained an instrumented 7-in. sphere for air density measurement equipped with accelerometer and telemetering. The second system employed a single tube in the Cajun nose cone for forward deployment of a single inflatable sphere. In this system, the nose cone also carried the principal payload of the rocket, 11 grenades for the measurement of winds and temperature, an experiment of GSFC.

## I. DETAILS OF ROCKET FLIGHTS

Table I summarizes four rocket flights at Wallops Island, Va., two of which resulted in data which have been processed to obtain pressure, density, and temperature profiles.

Each of the sphere envelopes was manufactured by the GT Schjeldahl Co., which also provided the isopentane capsules for releasing inflation gas. Two sphere designs were used, 1-m-diam sphere with metallized internal corner reflector (see Fig. 3), and a 4-ft-diam sphere with metallized envelope. Studies of the radar characteristics of the two targets did not conclusively indicate which one should be selected, so both were tried. The corner reflector design has had extensive use in the ROBIN program directed by R. Leviton and J. Wright of the Air Force Cambridge Research Laboratories.

Figure 1 shows dual pods arranged on a Cajun tail for aft deployment. Each sphere envelope was tightly packed in its tube between staves of phenolic material. Envelope and staves were ejected through the end of the tube by a charge of black powder ignited 110 sec after launching by a pyrotechnic fuse. The ejection system was manufactured by the Zimney Corp. Rocket 10.50 carried one each of the two sphere designs. The two ejections were made at approximately the same time. The radar acquired the corner reflector, which was the larger target, and it was tracked until deflation at approximately 38-km altitude. The second sphere was then acquired but not tracked.

Rocket 10.50 also carried The University of Michigan 7-in. sphere equipped with accelerometer and telemeter.<sup>1</sup> This instrumentation was developed under the direction of H. F. Schulte; the work was supported by Air Force Cambridge Research Laboratories. The 7-in. sphere was ejected at approximately 48 sec at an altitude of 57 km. Upleg data as well as downleg data were obtained down to an altitude of 46 km, at which altitude the telemetered signal became too small for recovery of data. The difficulty was believed to be due to antenna breakdown caused by the formation of an ionized plasma at this altitude.

The second application of the inflatable sphere system was an integration with rocket-grenade payloads. The rocket grenade program is presently under the direction of W. Nordberg and W. Smith of the Goddard Space Flight Center. Wind and temperature are measured by the rocket-grenade system, which is based on the principle of sound propagation.<sup>2</sup> In the current version of this application, 12 grenades are carried in a Cajun nose cone. The grenades are ejected from the rocket and exploded at intervals on the upleg portion of the trajectory. The time of arrival of the sound at the ground is detected by an array of microphones. The grenade nose cone (see Fig. 2)

has nine short mortar barrels in the outer circle for small grenades and three long barrels in the center for large grenades. In the present application the sphere package replaced one of the large grenades. The design and testing of the sphere package for the grenade payload was done under the direction of H. F. Allen of our laboratory.

Difficulties were encountered with sphere deployment on the first two flights. On 9-16-1961 the sphere was tracked but was apparently in an uninflated condition. On 3-23-1962 the sphere was not acquired by the radar. The apparent source of trouble in both flights was failure of the gas capsule to release isopentane. The capsule release mechanism was modified and a successful deployment was achieved from Rocket 10.43 on 6-6-1962. The grenade system telemetering failed on this flight but it was possible to recover the information needed for grenade data reduction from radar data. The sphere in this case was again the corner reflector design. No data were obtained for the metallized sphere design.

## II. DATA ANALYSIS PROCEDURES

The aerodynamic drag equation is fundamental to the falling sphere system for air density measurement:

$$D = \frac{A}{2} (C_D \rho) V^2 \quad (1)$$

The velocity  $V$  in Eq. (1) is the velocity of the sphere relative to the air through which it falls. A method of deriving atmospheric density based on this equation for a sphere falling through still air will now be developed.

The energy dissipated by drag on a sphere falling from upper altitude  $z_u$  to lower altitude  $z_l$  may be found by integrating drag force, Eq. (1), with respect to distance along the trajectory:

$$\Delta E = \int_{s_u}^{s_l} D ds = \int_{s_u}^{s_l} \frac{A}{2} (C_D \rho) V^2 ds \quad (2)$$

On the other hand, energy dissipated can be equated to the change of the sum of kinetic energy and potential energy of the sphere between altitude  $z_u$  and  $z_l$ :

$$\Delta E = m(\Delta PE + \Delta KE) \quad (3)$$

In Eq. (3) both PE and KE are the energy per unit mass and  $m$  is the mass of the sphere. These equations are used to compute mean value of the product of drag coefficient and air density between appropriately chosen levels  $z_u$  and  $z_l$ :

$$\Delta E = \int_{s_u}^{s_l} \frac{A}{2} (C_D \rho) V^2 ds = \frac{A}{2} \overline{C_D \rho} \int_{s_u}^{s_l} V^2 ds = \frac{A}{2} \overline{C_D \rho} \overline{V^2} \Delta s \quad (4)$$

where

$$\overline{V^2} = \frac{1}{2}(V_u^2 + V_l^2) \quad (5)$$

$$\Delta s = \overline{V} \Delta t, \quad \overline{V} = \frac{1}{2}(V_u + V_l) \quad (6)$$

The mean square velocity given by Eq. (5) is exact when acceleration is con-

- stant; when it is not constant,  $\Delta z$  should be sufficiently small to insure a satisfactory approximation. The density formula is derived from Eqs. (3) through (6):

$$\overline{C_D \rho} = \frac{2m}{A} \frac{\Delta PE + \Delta KE}{\overline{V^2 \Delta t}} \quad (7)$$

In the presence of a force due to gravity the change of potential energy per unit mass is equal to the force,  $g$ , times the change of altitude. The buoyant force is also vertical; consequently its effect on the sphere's motion can be accounted for by an additional term in the potential energy formula. The buoyant force is equal to the mass of air displaced by the sphere times the local value of gravity acceleration. The formula for change of potential energy then becomes

$$\begin{aligned} \Delta PE &= \left( \bar{g} - \frac{\bar{\rho}_g V_s}{m} \right) \Delta z \\ &= \bar{g} \Delta z \left( 1 - \frac{\bar{\rho}}{\rho_s} \right) \end{aligned} \quad (8)$$

where  $\rho_s$  is the mass per unit volume of the sphere. Buoyancy is an important effect only at the lowest altitude, where air density becomes as large as 8% of sphere density. Since air density appears on each side of Eq. (7), iterations are required. Gravity acceleration at altitude is derived from gravity at zero altitude by the inverse square law:

$$g = g_0 \left( \frac{r_e}{r_e + z} \right)^2 \quad (9)$$

where  $r_e$  is the earth's radius.

The drag coefficient  $C_D$  is a function of two aerodynamic parameters: Mach Number and Reynolds Number. In order to compute atmospheric density profiles  $C_D$  data are needed over a wide range of Reynolds Numbers and subsonic and supersonic Mach Numbers. The sources of these data are discussed in Appendix A.

The application of Eq. (7) involves double differentiation of radar position data since the derivation of velocity requires one differentiation and a second is involved in  $\Delta KE$ .

Velocity is derived by a least-squares fit of a parabola to each of the radar coordinates—range, azimuth, and elevation, which are functions of time. The extent of the data used to determine velocity was defined by the altitude

parameter  $\Delta z_v$ . The spacing of the energy levels  $z_u$  and  $z_l$  is defined by the altitude parameter  $\Delta z_e$ . Different values of  $\Delta z_v$  and  $\Delta z_e$  are used at different altitudes. The proper choice of values was studied in some detail and is described in Appendix B. Altitude was preferred over time as a smoothing parameter since its physical significance is more readily interpreted. The ability of the system to resolve fine-detail atmospheric structure may be improved at the expense of increased scatter by decreasing the amount of smoothing. It was felt that an appropriate amount of smoothing could best be chosen through a consideration of the altitude and altitude interval. Since the sphere velocity varies so widely in different parts of the trajectory, the specification of time interval was thought to be a less satisfactory approach.

The FPS-16 radar data were provided at a rate of 10 data points per second. At low altitude the sphere falls at a slower speed so that a larger number of data points appears within a given altitude interval; therefore more data were available than were needed. Since a considerable amount of computer memory is required for storage, the data were condensed by taking 1/2-sec averages of the 1/10-sec data below 57 km.

Equation (7) was used to compute a list of values for  $C_{Dp}$  at approximately 1-km levels from the lower level, where the sphere was collapsed, to the highest level where results could be obtained. The precise level of the  $C_{Dp}$  determination was the level of the radar data point which fell nearest an integer kilometer altitude, the difference being at most 50 m.

Drag coefficient  $C_D$  was then found by entering the drag coefficient function with Mach Number  $M$  and the product of drag coefficient and Reynolds Number  $C_{DRe}$

$$M = \frac{V}{c} \quad (10)$$

and

$$C_{DRe} = \frac{(C_{Dp})Vd}{\mu} \quad (11)$$

The speed of sound  $c$  and the viscosity  $\mu$  were derived from U.S. Standard Atmosphere, 1962. Using the drag coefficient found in this way, a list of density values at approximately 1-km levels was derived. The pressure at each kilometer level was then found by integrating the barometric equation

$$\Delta P = -\bar{\rho}g\Delta z \quad (12)$$

The mean density between levels  $z_n$  and  $z_{n+1}$  was calculated using the logarithmic formula

$$\rho = \frac{\rho_{n+1} - \rho_n}{\ln \frac{\rho_{n+1}}{\rho_n}} \quad (13)$$

The integration was downward from the highest level of 110 km where the pressure was assumed to be zero. A temperature profile was then derived using the gas equation of state

$$T = \frac{M^*p}{R^*p} \quad (14)$$

Where  $R^*$  is the universal gas constant and  $M^*$  is the molecular weight also assumed to be constant. Except at the highest levels, the temperature profile obtained in this way was believed to be a better source of speed of sound and viscosity data than U.S. Standard Atmosphere, 1962, which was used in the first determination of  $C_D$ . Therefore iterations were performed. Above 90-km altitude, Standard Atmosphere temperature was used; for altitudes between 40 and 90 km the derived temperatures averaged over 4 km were used; and below 40-km altitude the derived temperatures were used without being averaged. Iterated drag coefficient, density, pressure, and temperature profiles were then computed. Iterations were continued until the largest temperature change at any level was smaller than 1°K.

The influence of atmospheric wind on the sphere trajectory depends on altitude. In order to discuss wind and other factors it is useful to define (roughly) three regimes of the trajectory of a lightweight sphere falling from a maximum altitude of 150 km:

1. High altitude. Above about 95 km drag accelerations are less than 1 g. Above about 80 km, velocity is greater than twice the sound speed. Maximum Mach Number is 3.7 at about 95 km. Subsonic velocity occurs only at an extremely high altitude, where the system is insensitive to air density.
2. Middle altitude. Maximum drag acceleration is about 4.5 g at about 80 km. Sonic Mach Number occurs at about 70 km.
3. Low altitude. Below 70 km drag force and gravity force are approximately equal. The velocity is subsonic.

The second sphere deployed from the lower altitude of 120 km follows a similar pattern. More specific details of the two trajectories are plotted in Figs. 4, 5, 6, and 7.

In the high altitude regime the sphere velocity is large compared with expected atmospheric wind velocity. At the more extreme high altitudes gravity has a greater influence on the trajectory than the drag force. At high altitude, therefore, the sphere is not a useful sensor of winds, and the

total velocity of the sphere is used in the density formula [Eq. (7)].

At low altitude, the lightweight sphere tends to be carried along by horizontal wind so that the relative horizontal wind tends to become zero. For this regime, therefore, the vertical component of sphere velocity is used in the density formula [Eq. (7)].

The vertical component of velocity is calculated by the formula

$$\dot{z} = \dot{r} \cos \beta + r \dot{\epsilon} \sin \beta \quad (15)$$

where  $\beta$  is the angle between radar line of sight and vertical at the sphere.

$$\beta = \sin^{-1} \frac{\cos \epsilon}{1 + \frac{z}{r_e}} \quad (16)$$

where  $r_e$  is the earth's radius.

Table II shows that there is a relatively broad range of altitude in which either method is applicable since the total velocity and vertical component differ by less than 1%. The favorable geometry is due to the large drag accelerations, which tend to annihilate the horizontal motion and leave the sphere in a vertical trajectory. Although the lightweight sphere is a useful sensor of horizontal winds, the analysis of winds on these two spheres is incomplete and is not reported at this time. The presence of variable horizontal winds has a slight influence on the vertical motion of the sphere. This effect is discussed in Appendix C. At low altitude, the influence of vertical wind on the motion of the sphere is larger and cannot, unfortunately, be separated from density effects. The error in density measurements due to vertical wind depends on sphere velocity and is also discussed in Appendix C.

### III. DISCUSSION OF THE PROCESSED DATA

In Fig. 8 the density profiles derived from flights 10.50 and 10.43 are compared with those given in U.S. Standard Atmosphere, 1962. Tables III and IV exhibit the tabulated values. The smoothing parameter  $\Delta z_v$  was varied from 1 km at lowest altitude to 6 km at the highest altitude. The same variation of  $\Delta z_v$  was used for each flight. In each case  $\Delta z_e$  was made equal to  $\Delta z_v$ . No absolute standard for choosing smoothing parameters was found. As altitude increases, the derived density data tend to become more scattered. An increase of the smoothing parameter sufficient to control the scatter at the different altitudes was selected after examining the results of alternate choices. Some general considerations applicable to the choice of smoothing parameters are discussed in Appendix B, and specific examples are given.

The density profiles showed no radical departures from those of the U.S. Standard Atmosphere, 1962 except at altitudes in the neighborhood of 105 to 110 km. At this extreme altitude it was felt that the system could not be relied upon because it lacked sensitivity to the small drag forces that perturb the trajectory.

It is of interest that the data yielded by the 10.43 sphere, which fell from a peak altitude of 120 km, were comparable to those yielded by the 10.50 sphere which fell from a peak altitude of 150 km.

At low altitude, the sphere finally descends to a level where the ambient pressure is greater than the internal pressure maintained by the isopentane gas. A collapsed sphere appears to have much greater drag than a filled sphere, so that there is a sharp departure from the normal density profile. This departure can be readily seen on the plots. A second indication of collapse appears on the chart of radar automatic gain control voltage (see Fig. 9). The chart of an inflated sphere whose reflector is erect has a characteristic pattern. Smooth and irregular portions alternate as the sphere rotates and changes its aspect with respect to the radar. At 500 sec, the 10.50 sphere can be seen rotating at a faster rate than the 10.43 sphere. When the sphere has collapsed, an irregular pattern is always seen. The automatic gain control (AGC) charts indicate deflation at 770 and 970 sec for Flights 10.50 and 10.43 respectively; these values agree well with the break that appears on each density profile. Figure 9 shows the AGC trace for each of the two spheres when normally inflated and when deflation is believed to occur. It should be noted that deflation time need not be pinpointed very closely in order to get good results since an error of the order of 40 sec when the sphere rate of descent is 25 m/sec results in an error of only 1 km for altitude of deflation. The AGC method has the advantage of being independent of aerodynamic effects. If the sphere were caught in a severe gust of vertical wind, the calculated density profile might be sufficiently distorted as to be unreliable.

Flight 10.50 also carried a 7-in. sphere equipped with accelerometer and telemeter. This sphere instrumentation which is described in Ref. 1, is similar to the instrumentation described in Ref. 3 except that basic changes in accelerometer design and data encoding were made in an effort to improve sensitivity to small accelerations. The data were processed by the methods reported in Ref. 3, except that the new drag coefficient data reported in Ref. 4 were used. The processed data for the 7-in. sphere are shown in Tables V and VI. The density profile derived from the 7-in. sphere (see Fig. 8) shows an increasing departure from the standard atmosphere as altitude increases. The data appear to be abnormal. There were no indications of malfunction of the sphere instrumentation that would influence acceleration measurement. Unfortunately, two other spheres of this design were lost due to rocket vehicle failures. Since the 7-in. sphere was the only one of its design to perform in flight, the data associated with it do not have the validity of those associated with a proven system.

In Fig. 10 the temperature profiles derived from Flights 10.50 and 10.43 are compared with those given in U.S. Standard Atmosphere, 1962. The temperature profile derived directly from the density and pressure profiles shows some scattered data. Average temperatures are also plotted from the derivation of an arithmetic average of five temperatures bounding a 4-km layer.

Also plotted in Fig. 10 are the temperatures derived from the grenade payload of Flight 10.43. Eleven grenade explosions spaced at approximately 5-km levels yielded the ten average temperature points ranging from 46 to 93 km. The sphere-derived temperatures from 46 to 60 km are 10 to 20° higher than the grenade temperatures. From 69 to 85 km the agreement is better. The sphere data points are spaced closely enough to permit measurement of fine structure such as the minor temperature maximum at 78 km.

#### IV. ACKNOWLEDGMENTS

We are indebted to the Office of Space Sciences of the National Aeronautics and Space Administration for encouragement and for the financial support of the sphere program. We also wish to thank the personnel of NASA's Wallops Island Station who assisted in the flights.

## APPENDIX A

### SOURCES OF $C_D$ DATA

The drag coefficient of a sphere depends upon two aerodynamic parameters: Reynolds Number and Mach Number. Figure 11 is a plot which shows how these parameters vary in the trajectories of the two inflated 1-m spheres of Flights 10.50 and 10.43, and in the trajectory of the 7-in. instrumented sphere of Flight 10.50. At high altitude, where the Mach Number of the inflated spheres is supersonic, measurements of drag coefficient show little if any effect of Mach Number. The recent measurements of Ashkenas<sup>5</sup> and Ashkenas and Wegener<sup>6</sup> were especially relied upon for the supersonic drag coefficients used for sphere data processing. Figure 12 shows the measurements reported in Ref. 5; the curve drawn through these data is the one selected by the present writers for the purpose of sphere data processing.

At low altitude the motion of the sphere becomes subsonic. In this regime, very extensive falling-sphere measurements have been made with the ROBIN system developed by Air Force Cambridge Research Laboratories under the direction of R. Leviton and J. Wright. Determinations of drag coefficients for this program have been made by H. Heinrich.<sup>7</sup> Important Mach Number variations are indicated in this regime.

The supersonic and subsonic drag coefficient functions derived from these sources are believed to be quite accurate. In the transition area from subsonic to supersonic Mach Number, the drag coefficient increases by a factor of two. Unfortunately, data for this area are more scanty. The measurements made by A. May<sup>8</sup> at low supersonic Mach Numbers were used here. Fortunately, the transonic Mach Numbers occur in a relatively narrow range of altitude near 70 km.

The Mach Number and Reynolds Number are defined by the equations

$$M = \frac{V}{c} \quad (A-1)$$

$$Re = \frac{\rho V d}{\mu} \quad (A-2)$$

In the case of falling spheres, the unknown quantities are speed of sound  $c$ , density  $\rho$ , and viscosity  $\mu$ , since the velocity  $V$  is derived from radar data and the sphere diameter  $d$  is known. Density and viscosity can be found for Eq. (A-2) by an iterative procedure. An alternative scheme is to introduce the new dimensionless parameter  $C_D Re$  defined by

$$C_D Re = \frac{(C_D \rho) V a}{\mu} \quad (A-3)$$

The product  $C_D \rho$  can be derived directly from the radar data and a fair approximation to the viscosity can be derived from a standard atmosphere table. If more precise values of  $c$  and  $\mu$  are needed, iterations are required. The parameter  $C_D Re$  was used in the present data processing. All  $C_D$  data were cross-plotted in order to introduce  $C_D Re$  in place of  $Re$ . Table VII defines the  $C_D$  function. Linear interpolation was used to derive drag coefficient at any Mach Number and Reynolds Number.

## APPENDIX B

### CHOICE OF SMOOTHING PARAMETERS

A number of general considerations govern the proper choice of the two smoothing parameters  $\Delta z_v$  and  $\Delta z_e$ , which must be specified when the energy method is used in calculating air density. In the low range of altitudes, the choice was not difficult since 1-km values of  $\Delta z_v$  and  $\Delta z_e$  were sufficiently large so that the scatter was not severe. On the other hand, the 1-km value is sufficiently small to reveal fine structure of the atmosphere.

At high altitude, the smoothing must be increased in order to suppress scatter in the processed data. Some criterion of a reasonable upper limit is needed.

Atmospheric density profiles are, of source, approximately exponential. In this case the density is given by the formula

$$\frac{\rho}{\rho_0} = e^{\frac{z_0 - z}{H}} \quad (B-1)$$

where  $H$  is the scale height. Typical values of scale height in the atmosphere, which depend on the temperature, are 5 to 8 km. It is of interest to compare the average density  $\bar{\rho}$  over an altitude interval  $\Delta z$  with the density  $\rho_0$  at the center of the interval. The ratio, derived from Eq. (B-1) is given by the following formula:

$$\frac{\bar{\rho}}{\rho_0} = \frac{2H}{\Delta z} \sinh \left( \frac{\Delta z}{2H} \right) \quad (B-2)$$

Figure 13 is a plot of Eq. (B-2), which shows that if  $\Delta z = H$ ,  $\bar{\rho}$  exceeds  $\rho_0$  by about 4%. When data are recovered from trajectory analysis, the product  $C_D \rho$  rather than  $\rho$  is measured. Since the variability of  $\rho$  is much greater than the variability of  $C_D$ , the product  $C_D \rho$  is also approximately exponential so that Fig. 13 is applicable. An exception to this rule is near Mach Number 1 where  $C_D$  changes quite rapidly. It was decided that at high altitude, smoothing parameters as large as one scale height could be used.

The sphere velocity can be found by resolving three orthogonal components associated with the radar coordinates range, elevation angle, and azimuth angle.

$$V_r = \frac{dr}{dt}$$

$$V_e = r \frac{d\epsilon}{dt} \quad (B-3)$$

$$V_\alpha = r \cos \frac{d\alpha}{dt}$$

Each of the angle derivatives were found by a least-squares fit of a second-degree polynomial to the position data using all the data within the altitude interval  $\Delta z_v$  centered at the required altitude. For deriving range component of velocity, an altitude range of  $1/2 \Delta z_v$  was used. The smaller altitude interval was selected because the FPS-16 range data are more precise than the angle data, particularly at long range. Accuracy specifications often quoted for this radar are 5 yards in range and 1/10-mil in angle. These specifications imply that the range component of position error is independent of range, that the angle component of position error is proportional to range, and that the two are equal at a range of 50,000 yds. The range of the sphere at the altitude where greatest smoothing is required is more than 100,000 yds. On this basis, the smaller value of  $1/2 \Delta z_v$  was selected for the range component.

In order to study the effect of the  $\Delta z_v$  parameter on the derived velocities, data from Flight 10.50 were examined in detail at two specific altitudes: 80 km, where the drag is largest, and 105 km where the drag is small. The frequency of the data was 10 data points per second in both cases. Figure 14 shows that the velocity changes little for a wide range  $\Delta z_v$ . A practical minimum value for  $\Delta z_v$  at 80 or 105 km would appear to be somewhat greater than 1 km. The sphere falls quite rapidly at these altitudes so that only 8 or 10 data points are provided by the radar in 1-km altitude interval. Figures 15 and 16 are similar plots in which the range and elevation angle components of velocity are shown. The azimuthal component of velocity is very small at 80 and 105 km. Figures 17 and 18 show how the computed values of  $C_{D0}$  vary with the parameters  $\Delta z_v$  and  $\Delta z_e$  at altitudes of 80 and 105 km.

The final choice of  $\Delta z_v$  and  $\Delta z_e$  as a function of altitude was made after examining several density profiles computed using different values for these parameters.

## APPENDIX C

### EFFECTS OF WINDS

Analysis of the motion of a sphere falling through still air of constant density and velocity  $\dot{z}$  into a layer of uniform horizontal wind  $w$ , although a simplification, will yield a number of points of interest. Above the shear layer the drag is

$$D = \frac{1}{2} AC_D \rho \dot{z}^2 \quad (C-1)$$

Below the shear layer, the drag is larger and is inclined from the vertical an angle  $\delta$ :

$$D = \frac{1}{2} AC_D \rho [\dot{z}^2 + (w - \dot{x})^2] \quad (C-2)$$

$$\cos \delta = \frac{\dot{z}}{\sqrt{\dot{z}^2 + (w - \dot{x})^2}} \quad (C-3)$$

where  $\dot{x} = 0$  when  $t = 0$ . The vertical component of drag is

$$D \cos \delta = \frac{1}{2} AC_D \rho \dot{z} \sqrt{\dot{z}^2 + (w - \dot{x})^2} \quad (C-4)$$

The effect of a horizontal component of relative wind is therefore to increase the vertical component of drag. If the wind is small compared with the rate of descent of the sphere, the change of drag will be small since the function is a square root of the sum of squares. For example, a horizontal wind component of 14% of  $\dot{z}$  is required to increase the vertical component of drag by 1%. In addition, the perturbation on the vertical drag is a transient condition that tends toward zero as the sphere responds to the horizontal wind. Horizontal components of drag force and acceleration are equated in order to derive the transient equation

$$\begin{aligned} m\ddot{x} &= \frac{1}{2} AC_D \rho \sqrt{\dot{z}^2 + (w - \dot{x})^2} \cdot (w - \dot{x}) \\ &\cong \frac{1}{2} AC_D \rho \dot{z} (w - \dot{x}) \end{aligned} \quad (C-5)$$

The time constant of this first-order equation in  $\dot{x}$  is seen to be

$$t_c = \frac{2m}{AC_D \rho \dot{z}} \quad (C-6)$$

Below about 70-km altitude, where wind effects are most important, the equation for time constant can be simplified by the approximate equation

$$mg = \frac{A}{2} C_D \rho \dot{z}^2 \quad (C-7)$$

Equation (C-6) becomes

$$t_c = \frac{\dot{z}}{g} \quad (C-8)$$

The change of altitude associated with the time constant is

$$\Delta z_c = \dot{z} t_c = \frac{\dot{z}^2}{g} \quad (C-9)$$

Below 70-km altitude and above the altitude of sphere deflation,  $\dot{z}$  varies from about 250 m/sec to 20 m/sec; therefore the time required for relative horizontal wind to decay by a factor  $1/e$  varies from about 25 sec to about 2 sec. The altitude parameter  $\Delta z_c$  varies from 6 km to 40 m. It is believed that only an extraordinary field of horizontal wind would lead to significant errors in the computed density.

The effect of vertical wind on the determination of air density can be seen by considering the drag equation for a vertically falling sphere:

$$D = \frac{1}{2} AC_D \rho \dot{z}^2 \quad (C-10)$$

By differentiation,

$$\frac{dD}{D} = \frac{dC_D}{C_D} + \frac{d\rho}{\rho} + 2 \frac{d\dot{z}}{\dot{z}} \quad (C-11)$$

For small errors, then, the percent error in density is the same as the percent error in drag coefficient, and is double the percent error in vertical velocity. If the error in vertical velocity is due to an unknown vertical

- wind component  $w_z$ , then  $\dot{dz} = w_z$ . At high altitude where the sphere falls at a rate of 1000 m/sec, the density error due to a 1-m/sec vertical wind is 0.2%. At 70 km and 30 km, the errors are 0.8% and 10% for typical sphere velocities. If large vertical wind velocities are present and persist over a broad range of altitude, the possibility of a significant distortion of the derived density profile is present. At higher altitude, where larger vertical winds might be expected, the large sphere velocity tends to decrease errors due to wind.

## REFERENCES

1. Schulte, H. F., D. A. Robinson, and J. L. Wagener, Falling-sphere experiment for upper-air-density: instrumentation developments. The University of Michigan, Final Report ARCRL-62-662, 03558-6-F, 1962.
2. Nordberg, W., and W. G. Stroud, Results of IGY rocket-grenade experiments to measure temperature and winds above the island of Guam, J. Geophys. Research, 66, 455-464, 1961.
3. Jones, L. M., J. W. Peterson, E. J. Schaefer, and H. F. Schulte, Upper-air densities and temperatures from eight IGY rocket flights by the falling-sphere method, IGY Rocket Report Series No. 5, 1959.
4. Jones, L. M., and J. W. Peterson, 1961 Review, Upper air densities and temperatures measured by the falling-sphere method, The University of Michigan, ARCRL-803, 03558-5-T, 1961.
5. Ashkenas, H. I., Sphere drag at low Reynolds Numbers and supersonic speeds, Jet Propulsion Laboratory Research Summary, No. 36-12, Vol. I, 1962.
6. Wegener, P. P., and H. Ashkenas, Wind tunnel measurements of sphere drag at supersonic speeds and low Reynolds Numbers, J. Fluid Mech. 10, 550-560, 1961.
7. Engler, N. A., Development of methods to determine winds, density, pressure, and temperature from the ROBIN falling balloon, Air Force Cambridge Research Laboratories, 1962.
8. May, A., Supersonic drag of spheres at low Reynolds Numbers in free flight, NAVORD, Report 4392, 1956.

TABLE I

NIKE CAJUN FLIGHTS, WALLOPS ISLAND, VA.

Rocket Number	Date	Time	Sphere Diameter	Sphere Mass	Altitude, km		Other Payload	Results
					Ejection	Peak		
10.50	6/6/1961	1648R	1 m	99.5 g	122	150	7-in. sphere	p,ρ,T profiles
10.36	9/16/1961	--	4 ft	--	-	-	grenades	Sphere not inflated
10.40	3/23/1962	--	1 m	--	-	-	grenades	No radar track
10.43	6/6/1962	1910R	1 m	117.8 g	103	120	grenades	p,ρ,T profiles

TABLE II

## VELOCITY RATIO VS. ALTITUDE

z	10.50			10.43		
	v	$\dot{z}$	$\dot{z}/v$	v	$\dot{z}$	$\dot{z}/v$
80	2296	2241	.976	1933	1873	.969
79	2104	2057	.978	1822	1774	.973
78	1869	1832	.980	1736	1694	.976
77	1662	1638	.986	1600	1561	.976
76	1453	1439	.990	1456	1430	.982
75	1235	1226	.993	1321	1307	.990
74	1061	1058	.997	1161	1152	.992
73	912	912	1.000	1017	1017	1.000
72	810	810	1.000	913	913	1.000
71	767	765	.998	826	824	.997
70	731	727	.996	799	793	.993
69	685	678	.990	751	742	.988
68	673	661	.983	743	731	.984
67	631	623	.988	705	692	.982
66	595	585	.983	687	671	.976
65	577	565	.979	644	629	.978

v - total velocity, fps

 $\dot{z}$  - vertical component, fps

TABLE III

## PROCESSED DATA, FLIGHT 10.50, 1-m SPHERE

NO ITERATION PERFORMED ABOVE 90 KM. UNSMOOTHED TEMPS USED BELOW 40 KM.

ALTIT	DENSITY	PRESSURE	TEMPERATURE	VELOCITY	MACH	CORE	CD
KM.	GM/CC.M/	MILIBARS	DEG. KELVIN RAW SMOOTH	F/SEC	NO.		
110	.00004	.000000	0 0	2979	2.81	8	3.494
109	.00003	.000004	38 0	3000	2.85	7	3.623
108	.00009	.000007	34 39	3036	2.92	16	2.857
107	.00013	.000021	41 65	3058	2.97	26	2.432
106	.00016	.000037	81 84	3090	3.03	24	2.478
105	.00014	.000052	130 115	3128	3.10	22	2.550
104	.00017	.000066	134 138	3156	3.16	21	2.409
103	.00015	.000082	191 155	3176	3.21	24	2.476
102	.00022	.000097	155 157	3202	3.28	34	2.241
101	.00026	.000123	163 155	3215	3.33	39	2.148
100	.00037	.000151	141 140	3239	3.39	53	1.979
99	.00055	.000197	126 136	3267	3.45	72	1.817
98	.00077	.000257	116 131	3278	3.48	96	1.689
97	.00088	.000331	131 131	3292	3.52	108	1.640
96	.00106	.000422	139 136	3302	3.56	127	1.578
95	.00132	.000541	143 146	3298	3.59	154	1.507
94	.00155	.000674	152 153	3303	3.62	177	1.460
93	.00175	.000824	165 156	3311	3.65	198	1.424
92	.00213	.001010	165 158	3294	3.67	235	1.380
91	.00293	.001252	155 162	3271	3.67	302	1.319
90	.00360	.001552	150 156	3243	3.95	421	1.262
89	.00399	.001932	169 151	3233	4.00	473	1.244
88	.00588	.002382	141 151	3172	3.92	657	1.199
87	.00756	.002997	138 158	3131	3.79	788	1.176
86	.00634	.003779	158 162	3083	3.69	833	1.169
85	.00676	.004597	183 171	2984	3.47	806	1.173
84	.01016	.005485	188 180	2858	3.24	852	1.167
83	.01199	.006541	190 183	2742	3.08	941	1.156
82	.01517	.007891	181 182	2616	2.95	1125	1.138
81	.01897	.009413	173 178	2483	2.83	1339	1.121
80	.02263	.011513	177 176	2295	2.63	1479	1.111
79	.02843	.013905	170 177	2096	2.39	1664	1.096
78	.03282	.016840	179 179	1895	2.16	1764	1.082
77	.03772	.020239	187 181	1671	1.89	1674	1.059
76	.04688	.024134	179 185	1467	1.64	1723	1.023
75	.05400	.029036	187 192	1272	1.40	1613	.988
74	.06187	.034603	195 193	1084	1.19	1508	.950
73	.06739	.040696	210 198	946	1.02	1353	.917
72	.08676	.048049	193 200	842	.91	1117	.866
71	.09700	.056767	204 198	769	.83	1021	.891
70	.11962	.067330	196 201	724	.78	1076	.844
69	.15020	.080136	186 203	688	.73	1186	.808
68	.14465	.094173	227 210	648	.68	1003	.486
67	.18742	.110152	205 219	616	.63	1148	.468
66	.18895	.128328	237 238	583	.57	1004	.459
65	.21128	.147216	243 243	558	.54	1045	.455
64	.20931	.167436	279 259	540	.51	942	.450
63	.26163	.190035	253 263	518	.49	1095	.442
62	.26287	.215366	285 273	492	.45	1008	.440
61	.32991	.243569	257 274	464	.43	1176	.433
60	.32773	.275381	293 279	439	.40	1085	.431
59	.38446	.309463	280 276	421	.39	1221	.428
58	.43728	.348908	278 278	393	.36	1286	.427
57	.50714	.394371	271 275	368	.34	1405	.427
56	.57969	.446097	268 276	339	.31	1475	.426
55	.63540	.506330	278 278	319	.29	1510	.426
54	.69221	.568780	286 281	304	.28	1558	.426
53	.77247	.638165	288 284	288	.26	1639	.427
52	.87628	.713649	286 282	271	.25	1757	.427
51	1.00714	.810042	280 281	252	.23	1886	.428
50	1.17198	.913910	272 280	233	.21	2040	.429
49	1.29430	1.034833	279 278	218	.20	2130	.430
48	1.44004	1.164706	282 277	208	.19	2271	.432
47	1.64620	1.310366	277 277	194	.18	2433	.434
46	1.35990	1.482867	278 276	181	.17	2590	.436
45	2.15760	1.675631	271 274	168	.15	2818	.438
44	2.43163	1.897367	272 272	157	.14	2997	.440
43	2.73504	2.150584	274 270	148	.14	3213	.443
42	3.16779	2.429527	267 268	137	.13	3474	.446
41	3.61219	2.757994	266 263	127	.12	3707	.449
40	4.18540	3.145530	262 254	118	.11	4189	.453
39	5.03837	3.584469	248 237	106	.10	4701	.458
38	6.29106	4.135129	229 213	94	.09	5646	.465
37	9.30749	4.872131	182 190	76	.09	8444	.479
36	14.62074	6.006366	143 175	59	.07	12978	.489
35	17.72509	7.578454	149 167	53	.07	13601	.489
34	19.06564	9.386127	172 0	51	.06	17334	.488
33	20.64552	11.297326	191 0	48	.05	11631	.487

TABLE IV

## PROCESSED DATA, FLIGHT 10.43, 1-m SPHERE

NO ITERATION PERFORMED ABOVE 90 KM. UNSMOOTHED TEMPS USED BELOW 40 KM.

ALTIT	DENSITY	PRESSURE	TEMPERATURE	VELOCITY	MACH	CDRE	CD
KM.	GM/CM <sup>3</sup>	MILIBARS	DEG. KELVIN RAW SMOOTH	M/SEC	NO.		
110	.00009	.000000	0 0	1640	1.54	9	3.386
109	.00011	.000009	29 0	1699	1.61	11	3.165
108	.00010	.000019	67 67	1757	1.69	11	3.198
107	.00007	.000028	130 92	1817	1.76	9	3.390
106	.00012	.000037	107 110	1868	1.83	13	3.007
105	.00013	.000049	129 111	1914	1.90	15	2.915
104	.00019	.000064	117 112	1961	1.96	20	2.625
103	.00044	.000092	72 119	1998	2.02	39	2.143
102	.00034	.000129	133 123	2052	2.10	33	2.259
101	.00040	.000163	143 134	2102	2.18	39	2.151
100	.00047	.000205	150 158	2141	2.24	46	2.054
99	.00052	.000253	170 174	2180	2.30	50	2.002
98	.00055	.000304	192 178	2216	2.36	54	1.965
97	.00057	.000355	216 177	2238	2.40	57	1.940
96	.00092	.000428	161 174	2278	2.46	85	1.743
95	.00125	.000530	147 168	2310	2.51	110	1.632
94	.00150	.000661	154 155	2333	2.56	130	1.569
93	.00177	.000820	161 153	2357	2.60	152	1.511
92	.00234	.001005	150 154	2371	2.64	193	1.432
91	.00287	.001264	154 158	2376	2.67	233	1.383
90	.00362	.001560	150 155	2382	2.91	324	1.307
89	.00387	.001915	172 154	2400	2.94	347	1.294
88	.00557	.002381	149 156	2385	2.91	473	1.244
87	.00708	.002966	146 158	2369	2.87	577	1.216
86	.00793	.003667	161 157	2343	2.84	636	1.203
85	.00989	.004527	160 163	2305	2.74	740	1.183
84	.01141	.005556	170 169	2241	2.62	799	1.174
83	.01304	.006697	179 174	2183	2.52	859	1.166
82	.01617	.008111	175 182	2107	2.37	973	1.147
81	.01805	.009722	188 192	2027	2.23	992	1.139
80	.02008	.011526	200 197	1937	2.10	1023	1.130
79	.02184	.013579	217 199	1837	1.98	1033	1.117
78	.02627	.015823	205 200	1714	1.84	1152	1.091
77	.03528	.018792	186 197	1603	1.74	1389	1.058
76	.04043	.022420	193 190	1466	1.62	1472	1.035
75	.05037	.026805	185 188	1317	1.46	1604	1.001
74	.06207	.032174	181 194	1177	1.28	1654	.963
73	.06751	.038277	198 197	1045	1.13	1531	.934
72	.07329	.045227	215 198	927	1.00	1423	.906
71	.08898	.052762	207 199	854	.92	1233	.705
70	.11319	.062436	192 211	785	.82	1139	.585
69	.14050	.074663	185 212	742	.77	1234	.542
68	.11798	.086812	256 219	717	.74	923	.513
67	.15722	.099973	222 225	700	.71	1139	.498
66	.16912	.115864	239 238	668	.66	1071	.478
65	.21004	.133689	222 237	634	.63	1233	.465
64	.21286	.154081	252 245	600	.58	1138	.459
63	.24529	.176252	250 250	573	.55	1215	.454
62	.26938	.200844	260 261	543	.51	1204	.446
61	.29790	.227981	267 263	517	.48	1238	.440
60	.32570	.258158	276 270	492	.46	1253	.436
59	.38506	.292062	264 273	464	.43	1371	.432
58	.40321	.329832	285 275	438	.40	1338	.429
57	.47436	.372356	273 275	414	.38	1480	.426
56	.52654	.419587	278 278	388	.35	1526	.426
55	.60321	.475216	274 277	363	.33	1637	.427
54	.66610	.534911	280 279	341	.31	1691	.427
53	.74447	.602953	282 281	322	.29	1777	.427
52	.83501	.678021	283 281	303	.28	1882	.428
51	.93288	.765822	286 281	285	.26	1978	.428
50	1.10788	.865000	272 280	263	.24	2186	.431
49	1.20715	.973509	281 280	246	.22	2234	.431
48	1.38367	1.097613	276 278	233	.21	2448	.434
47	1.52543	1.240621	283 280	218	.20	2514	.435
46	1.74985	1.398556	278 280	205	.19	2727	.437
45	1.93894	1.576430	283 279	192	.17	2852	.439
44	2.22806	1.778487	278 275	180	.16	3125	.442
43	2.58611	2.010547	271 273	165	.15	3376	.445
42	3.00675	2.278055	264 270	153	.14	3685	.448
41	3.35564	2.587347	269 267	143	.13	3916	.450
40	3.79961	2.935885	269 265	135	.13	4223	.453
39	4.43974	3.329899	261 264	124	.12	4621	.457
38	5.08949	3.795622	260 261	115	.11	4965	.460
37	5.78227	4.318292	260 256	107	.10	5286	.462
36	6.77239	4.930118	254 252	98	.09	5859	.467
35	8.01532	5.641495	245 245	90	.09	6562	.471
34	9.45873	6.484120	239 239	82	.08	7282	.475
33	11.51830	7.502120	227 234	73	.07	8349	.479
32	13.04915	8.686329	232 223	69	.07	8715	.480
31	15.52167	10.067806	226 0	63	.06	9705	.483
30	21.80934	11.860705	189 0	52	.06	13197	.489

TABLE V

## PROCESSED DATA, FLIGHT 10.50, 7-IN. SPHERE, UPLEG TRAJECTORY

Processed Data  
Seven Inch Sphere Flight 10.50  
Up Leg Trajectory

TIME SECONDS	DRAG ACCEL	VELOCITY VERTICAL	VELOCITY HORIZONTAL	ALTITUDE FEET	ALTITUDE METERS	DRAG COEFF.	DENSITY SL/CU FT	DENSITY KG/CU M.	PRESSURE LB/SQ FT	PRESSURE DYNES/CM <sup>2</sup>	TEMPERATURE F	TEMPERATURE C
189.76	.000		950.	494342.	150676.							
78.13	.088	3428.	980.	303550.	92522.	1.499	.00001067	.00000550				
77.35	.100	3453.	981.	300866.	91704.	1.465	.00001225	.00000631	.00744	3.564	-106.	-77.
76.62	.100	3475.	981.	298337.	90933.	1.466	.00001209	.00000623	.00840	4.021	-56.	-49.
75.97	.117	3496.	982.	296071.	90243.	1.434	.00001431	.00000737	.00933	4.468	-80.	-63.
75.30	.134	3517.	982.	293723.	89527.	1.412	.00001644	.00000848	.01045	5.009	-89.	-68.
74.52	.123	3541.	982.	290970.	88688.	1.428	.00001474	.00000750	.01181	5.652	7.	-14.
73.74	.190	3565.	983.	288198.	87843.	1.355	.00002370	.00001222	.01345	6.437	-130.	-90.
71.74	.187	3628.	984.	281005.	85650.	1.360	.00002249	.00001159	.01865	8.928	23.	-5.
71.31	.220	3642.	985.	279442.	85174.	1.333	.00002582	.00001382	.01985	9.505	-29.	-34.
68.12	.323	3742.	986.	267666.	81585.	1.271	.00003923	.00002022	.03191	15.279	14.	-10.
67.80	.365	3752.	987.	266467.	81219.	1.251	.00004483	.00002310	.03349	16.036	-25.	-32.
67.41	.365	3764.	987.	265001.	80772.	1.251	.00004454	.00002295	.03555	17.021	5.	-15.
67.05	.439	3776.	987.	263644.	80359.	1.219	.00005465	.00002877	.03766	18.030	-59.	-51.
66.69	.505	3787.	988.	262282.	79944.	1.196	.00005375	.00003286	.04019	19.240	-93.	-70.
66.32	.400	3799.	988.	260879.	79516.	1.237	.00004854	.00002502	.04255	20.419	52.	11.
65.97	.526	3810.	988.	259548.	79110.	1.190	.00005599	.00003401	.04503	21.593	-63.	-53.
65.34	.566	3830.	989.	257141.	78377.	1.178	.00007103	.00003661	.05021	24.038	-46.	-45.
64.94	.554	3842.	989.	255607.	77909.	1.182	.00005804	.00003548	.05358	25.653	-7.	-22.
64.58	.677	3854.	989.	254221.	77487.	1.147	.00006617	.00004441	.05694	27.264	-75.	-60.
64.25	.653	3864.	990.	252948.	77099.	1.154	.000068219	.00004236	.05031	28.878	-33.	-35.
63.88	.719	3876.	990.	251516.	76632.	1.138	.00009127	.00004704	.05422	30.746	-50.	-46.
63.53	.706	3887.	990.	250157.	76248.	1.141	.00008866	.00004580	.05807	32.589	-14.	-26.
63.07	.710	3902.	990.	248366.	75702.	1.142	.00008867	.00004570	.07307	34.984	20.	-7.
62.47	.682	3921.	991.	2465019.	74987.	1.107	.00011262	.00005804	.08047	38.527	-44.	-42.
62.06	.992	3934.	991.	244409.	74496.	1.094	.00012736	.00006564	.08654	41.436	-64.	-54.
61.76	.990	3944.	992.	243227.	74136.	1.095	.00012641	.00006515	.09126	43.695	-40.	-40.
61.46	1.031	3954.	992.	242042.	73774.	1.092	.00013139	.00006772	.09607	45.977	-34.	-37.
60.25	1.245	3993.	993.	237234.	72309.	1.077	.00015782	.00008134	.11791	55.452	-25.	-32.
59.55	1.301	4015.	994.	234431.	71455.	1.075	.00016351	.00008427	.13209	63.245	1.	-12.
58.90	1.502	4037.	994.	231814.	70657.	1.063	.00018893	.00009737	.14660	70.192	-8.	-22.
58.55	1.586	4048.	995.	230399.	70226.	1.059	.00019927	.00010267	.15526	74.336	-6.	-21.
58.32	1.690	4056.	995.	229467.	69942.	1.054	.00021259	.00010957	.16131	77.233	-18.	-28.
57.90	1.710	4070.	995.	227761.	69422.	1.054	.00021373	.0001016	.17278	82.728	1.	-12.
57.51	1.935	4083.	996.	226171.	68937.	1.043	.00024281	.00012514	.18421	88.199	-18.	-28.
57.16	1.945	4094.	996.	224740.	68501.	1.044	.00024268	.00012508	.19509	93.409	9.	-13.
56.78	1.967	4107.	997.	223182.	68026.	1.043	.00024403	.00012577	.20705	99.137	35.	1.
56.48	2.278	4117.	997.	221948.	67650.	1.031	.00028479	.00014678	.21733	104.055	-16.	-27.
56.20	2.291	4126.	997.	220794.	67298.	1.031	.00028514	.00014696	.22772	109.029	6.	-15.
55.69	2.429	4143.	998.	218685.	66655.	1.027	.00030117	.00015522	.24722	118.368	19.	-8.
54.67	2.829	4178.	999.	214442.	65362.	1.015	.00034923	.00017999	.29070	139.186	25.	-4.
54.31	3.072	4190.	1000.	212935.	64903.	1.008	.00037962	.00019565	.30802	147.480	13.	-11.
53.97	3.184	4202.	1000.	211508.	64468.	1.006	.00039235	.00020222	.32542	155.808	24.	-5.
52.14	4.238	4266.	1003.	203760.	62106.	.983	.00051882	.00026740	.43619	208.848	30.	-2.
51.87	4.374	4276.	1003.	202607.	61755.	.977	.00056118	.00028923	.45587	218.268	14.	-11.
50.90	5.335	4311.	1005.	198443.	60485.	.965	.00065239	.00033624	.53559	256.440	19.	-8.
50.54	5.387	4324.	1006.	196888.	60012.	.962	.00068190	.00035145	.56838	272.138	26.	-4.
50.00	5.752	4344.	1007.	194548.	59298.	.960	.00069666	.00035906	.61940	296.558	58.	15.
49.75	6.213	4353.	1008.	193461.	58967.	.953	.00075456	.00038890	.64434	308.511	38.	3.
49.42	6.793	4366.	1008.	192022.	58528.	.946	.00082698	.00042623	.68031	325.730	20.	-7.
49.02	7.202	4381.	1009.	190273.	57995.	.942	.00087506	.00045100	.72740	348.280	25.	-5.
48.68	8.759	4394.	1010.	188781.	57541.	.924	.00107788	.00055554	.77334	370.272	-42.	-41.
47.99	8.602	4422.	1012.	185739.	56613.	.927	.00104223	.00053716	.87539	419.135	30.	-2.

TABLE VI

## PROCESSED DATA, FLIGHT 10.50, 7-IN. SPHERE, DOWNLEG TRAJECTORY

Processed Data Seven Inch Sphere Flight 10.50 Down Leg Trajectory											
TIME SECONDS	DRAG ACCEL FT/SEC <sup>2</sup>	VELOCITY VERTICAL FT/SEC	VELOCITY HORIZONTAL FT/SEC	ALTITUDE HORIZONTAL FEET	ALTITUDE METERS	DRAG COEFF.	DENSITY SL/CU FT X1000	DENSITY KG/CU M.	PRESSURE LB/SQ FT	PRESSURE DYNES/SQ CM	TEMPERATURE F C
189.76	.000		950.	494342.	150676.						
302.66	.128	-3468.	981.	299168.	91187.	1.418	.00001607	.00000828			
303.38	.101	-3491.	981.	296663.	90423.	1.464	.00001213	.00000625	.01087	5.202	62.
304.06	.131	-3512.	982.	294283.	89697.	1.415	.00001609	.00000829	.01191	5.702	-29.
305.47	.142	-3555.	982.	289301.	88179.	1.404	.00001719	.00000886	.01451	6.946	32.
306.81	.194	-3597.	983.	284510.	86719.	1.352	.00002386	.00001230	.01757	8.409	-31.
307.92	.243	-3631.	984.	280499.	85496.	1.315	.00003019	.00001556	.02095	10.029	-56.
309.34	.290	-3675.	984.	275312.	83915.	1.287	.00003600	.00001856	.02632	12.602	-34.
310.02	.249	-3696.	985.	272806.	83151.	1.314	.00002995	.00001544	.02891	13.841	103.
311.13	.337	-3730.	985.	268685.	81895.	1.263	.00004144	.00002136	.03349	16.033	11.
311.51	.322	-3742.	986.	267265.	81463.	1.272	.00003910	.00002015	.03528	16.892	66.
311.94	.302	-3755.	986.	265654.	80971.	1.283	.00003609	.00001860	.03718	17.802	141.
312.50	.416	-3773.	986.	263546.	80329.	1.229	.00005149	.00002654	.04003	19.176	-7.
312.85	.386	-3783.	986.	262224.	79926.	1.242	.00004700	.00002423	.04210	20.154	62.
313.23	.384	-3795.	987.	260784.	79487.	1.244	.00004644	.00002393	.04420	21.164	95.
313.52	.480	-3804.	987.	259682.	79151.	1.205	.00005962	.00003073	.04603	22.039	-10.
313.91	.502	-3816.	987.	258197.	78698.	1.198	.00006237	.00003214	.04888	23.402	-4.
314.25	.514	-3827.	987.	256898.	78303.	1.194	.00006373	.00003285	.05146	24.637	11.
314.70	.476	-3840.	987.	255173.	77777.	1.208	.00005794	.00002986	.05475	26.215	91.
315.31	.639	-3859.	988.	252824.	77061.	1.158	.00008044	.00004146	.05982	28.640	-27.
315.69	.603	-3871.	988.	251356.	76613.	1.168	.00007478	.00003854	.06340	30.355	34.
316.03	.603	-3881.	988.	250038.	76212.	1.169	.00007438	.00003834	.06650	31.837	61.
316.78	.819	-3904.	988.	247119.	75322.	1.118	.00010442	.00005382	.07463	35.773	-44.
317.10	.876	-3914.	988.	245869.	74941.	1.108	.00011221	.00005783	.07889	37.773	-51.
317.44	.805	-3924.	989.	244537.	74535.	1.124	.00010111	.00005211	.08336	39.912	21.
317.80	.914	-3935.	989.	243122.	74104.	1.104	.00011634	.00005996	.08820	42.228	-18.
318.10	1.028	-3944.	989.	241940.	73743.	1.092	.00013168	.00006787	.09280	44.434	-50.
319.17	.977	-3977.	989.	237703.	72452.	1.099	.00012244	.00006310	.10975	52.548	63.
319.58	1.029	-3989.	989.	236070.	71954.	1.095	.00012863	.00006630	.11621	55.639	67.
319.90	1.039	-3999.	990.	234792.	71565.	1.095	.00012932	.00006665	.12140	58.125	87.
320.24	1.300	-4009.	990.	233431.	71150.	1.075	.00016397	.00008451	.12766	61.123	-7.
321.31	1.811	-4041.	990.	229125.	69837.	1.047	.00023105	.00011908	.15421	73.834	-71.
321.79	1.642	-4055.	990.	227182.	69245.	1.057	.00020611	.00010623	.16758	80.238	14.
322.13	1.856	-4065.	990.	225802.	68825.	1.047	.00023420	.00012071	.17715	84.819	-19.
322.36	2.010	-4072.	990.	224866.	68539.	1.040	.00025449	.00013116	.18436	88.271	-38.
322.71	2.125	-4082.	990.	223440.	68104.	1.036	.00026890	.00013859	.19613	95.908	-35.
323.47	2.322	-4104.	990.	220329.	67156.	1.029	.00029257	.00015084	.22367	107.094	-15.
323.71	2.359	-4111.	990.	219343.	66856.	1.028	.00029664	.00015289	.23284	111.483	-3.
324.14	2.625	-4124.	990.	217573.	66316.	1.019	.00033107	.00017063	.25036	119.872	-20.
324.84	2.676	-4144.	990.	214680.	65344.	1.019	.00033450	.00017240	.26075	134.424	29.
325.21	2.903	-4154.	991.	213145.	64967.	1.012	.00036351	.00018735	.29766	142.519	17.
325.56	3.114	-4164.	991.	211689.	64523.	1.007	.00039037	.00020120	.31498	150.814	10.
325.90	3.260	-4174.	991.	210272.	64091.	1.003	.00040832	.00021045	.33286	159.371	15.
326.23	3.522	-4183.	990.	208893.	63671.	.997	.00044212	.00022787	.35136	168.232	3.
326.50	3.602	-4191.	990.	207762.	63266.	.995	.00045130	.00023260	.36732	175.870	15.
326.99	3.904	-4204.	990.	205706.	62699.	.989	.00048930	.00025218	.39786	190.494	14.
327.32	4.196	-4213.	990.	204317.	62276.	.983	.00052694	.00027159	.42015	201.165	5.
327.65	4.294	-4222.	990.	202925.	61852.	.982	.00053788	.00027722	.44357	212.381	21.
327.99	4.570	-4232.	990.	201488.	61414.	.977	.00055303	.00029534	.46879	224.456	17.
328.34	4.864	-4241.	990.	200006.	60962.	.971	.00061051	.00031466	.49652	237.732	14.
328.73	5.057	-4251.	990.	198350.	60457.	.969	.00063363	.00032657	.52908	253.324	27.
329.35	5.641	-4268.	989.	195709.	59652.	.960	.00070821	.00036501	.58505	280.122	22.
329.83	6.014	-4280.	989.	193658.	59027.	.955	.00075482	.00038904	.63250	302.839	29.
330.18	6.508	-4289.	989.	192159.	58570.	.948	.00081931	.00042227	.66982	320.711	17.
330.57	6.939	-4298.	989.	190485.	58060.	.943	.00087463	.00045078	.71467	342.183	16.
330.93	7.110	-4307.	988.	188935.	57586.	.942	.00089418	.00046086	.75803	362.946	34.
331.22	7.513	-4314.	988.	187686.	57207.	.937	.00094653	.00048784	.79443	380.371	29.
331.44	8.192	-4320.	988.	186736.	56917.	.929	.00103812	.00053505	.82424	394.643	3.
332.22	8.955	-4338.	987.	183360.	55880.	.923	.00113424	.00058459	.94026	450.193	23.
332.56	9.501	-4345.	986.	181884.	55438.	.918	.00120377	.00062145	.99494	476.377	21.
332.94	10.321	-4354.	986.	180232.	54935.	.911	.00131516	.00067783	1.06086	507.937	10.
333.29	11.015	-4361.	985.	178706.	54470.	.906	.00140662	.00072497	1.12659	539.409	7.
333.69	11.641	-4369.	984.	176961.	53938.	.906	.00148138	.00076350	1.20042	577.635	15.
334.00	11.979	-4373.	984.	175606.	53525.	.906	.00152838	.00078361	1.27089	608.499	27.
335.09	13.797	-4396.	981.	170826.	52068.	.906	.00173595	.00089471	1.51716	726.414	50.
335.54	14.655	-4404.	980.	168846.	51464.	.906	.00183773	.00094718	1.62930	780.109	57.
337.12	22.356	-4425.	975.	161872.	49339.	.906	.00277938	.00143249	2.13271	1021.141	-13.
337.54	21.524	-4429.	974.	160013.	48772.	.906	.00267142	.00137685	2.29350	1098.126	41.
337.87	23.967	-4432.	972.	158551.	48326.	.906	.00297108	.00153130	2.42427	1160.739	16.
339.62	28.542	-4443.	963.	150787.	45960.	.906	.00352557	.00181708	3.22298	1943.162	73.

TABLE VII  
DRAG COEFFICIENT FUNCTION

M	C <sub>Dre</sub>																M ≥ 2.5 or z > 90 km C <sub>Dre</sub>	C <sub>D</sub>
	400	500	700	800	900	1000	1200	1500	2000	3000	5000	7000	10000	15000	20000	30000		
0-.39	.444	.444	.442	.438	.434	.432	.428	.426	.428	.440	.460	.474	.484	.491	.494	.497	12	3.08
.485	.442	.444	.444	.446	.446	.444	.440	.442	.443	.443	.460	.474	.484	.491	.494	.497	16	2.835
.53	.432	.444	.454	.456	.455	.453	.451	.450	.450	.450	.460	.474	.484	.491	.494	.497	20	2.62
.62	.447	.458	.468	.469	.468	.466	.463	.463	.463	.463	.463	.474	.484	.491	.494	.497	30	2.32
.685	.476	.486	.493	.492	.490	.488	.486	.486	.486	.486	.486	.486	.486	.491	.494	.497	40	2.13
.75	.499	.510	.519	.520	.519	.517	.516	.516	.516	.516	.516	.516	.516	.516	.516	.516	50	2.005
.80	.513	.532	.554	.560	.564	.566	.569	.572	.576	.582	.589	.594	.599	.605	.609	.615	70	1.83
.85	.544	.564	.587	.595	.600	.605	.610	.615	.620	.627	.636	.642	.648	.655	.660	.667	90	1.715
.90	.572	.592	.619	.628	.636	.642	.651	.661	.670	.676	.684	.690	.696	.702	.707	.714	100	1.67
.95	.816	.808	.800	.798	.795	.793	.788	.780	.771	.760	.747	.740	.734	.730	.730	.730	150	1.515
1.0	1.054	1.023	.982	.968	.954	.943	.924	.900	.874	.844	.811	.790	.772	.760	.753	.745	200	1.42
1.1	1.084	1.052	1.008	.994	.979	.969	.949	.927	.902	.870	.837	.817	.800	.785	.780	.777	300	1.32
1.2	1.110	1.077	1.033	1.019	1.004	.994	.975	.954	.929	.896	.861	.842	.824	.808	.801	.797	400	1.27
1.5	1.171	1.139	1.097	1.081	1.069	1.055	1.036	1.016	.989	.955	.920	.900	.883	.864	.856	.851	500	1.235
1.8	1.217	1.184	1.141	1.126	1.113	1.101	1.082	1.060	1.032	.999	.964	.945	.925	.906	.899	.895	700	1.19
2.1	1.250	1.219	1.175	1.160	1.145	1.133	1.113	1.090	1.065	1.034	.999	.977	.956	.943	.930	.920	900	1.16
2.5	1.270	1.235	1.190	1.179	1.160	1.150	1.130	1.110	1.085	1.050	1.015	.995	.970	.955	.950	.945	1000	1.15
																	1500	1.11
																	2000	1.085
																	3000	1.05
																	4000	1.03
																	5000	1.015
																	7000	.995
																	9000	.98
																	10000	.97
																	15000	.955
																	20000	.95
																	30000	.945

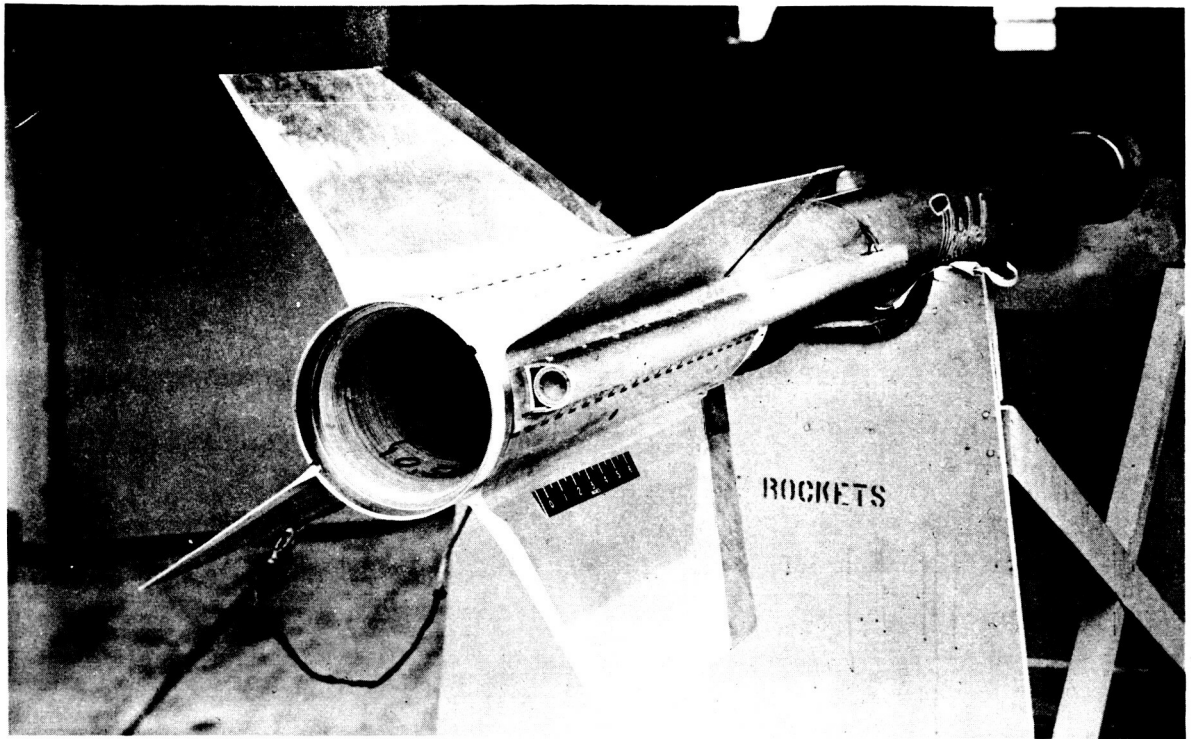


Fig. 1. Ejector pods on tail of Cajun.

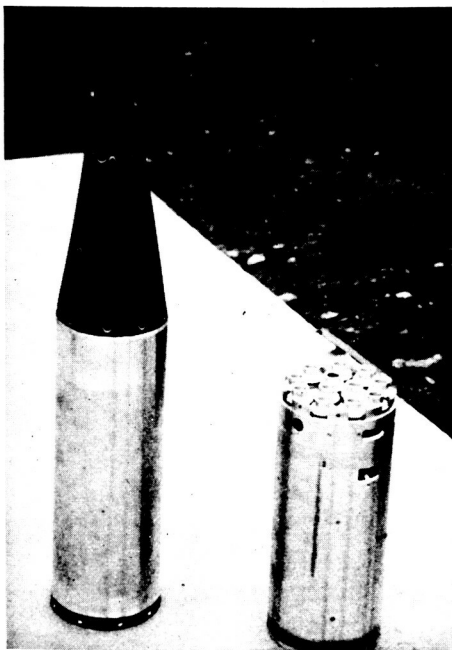


Fig. 2. Grenade Cajun nose cone, uncovered.



Fig. 3. One-meter corner reflector sphere.

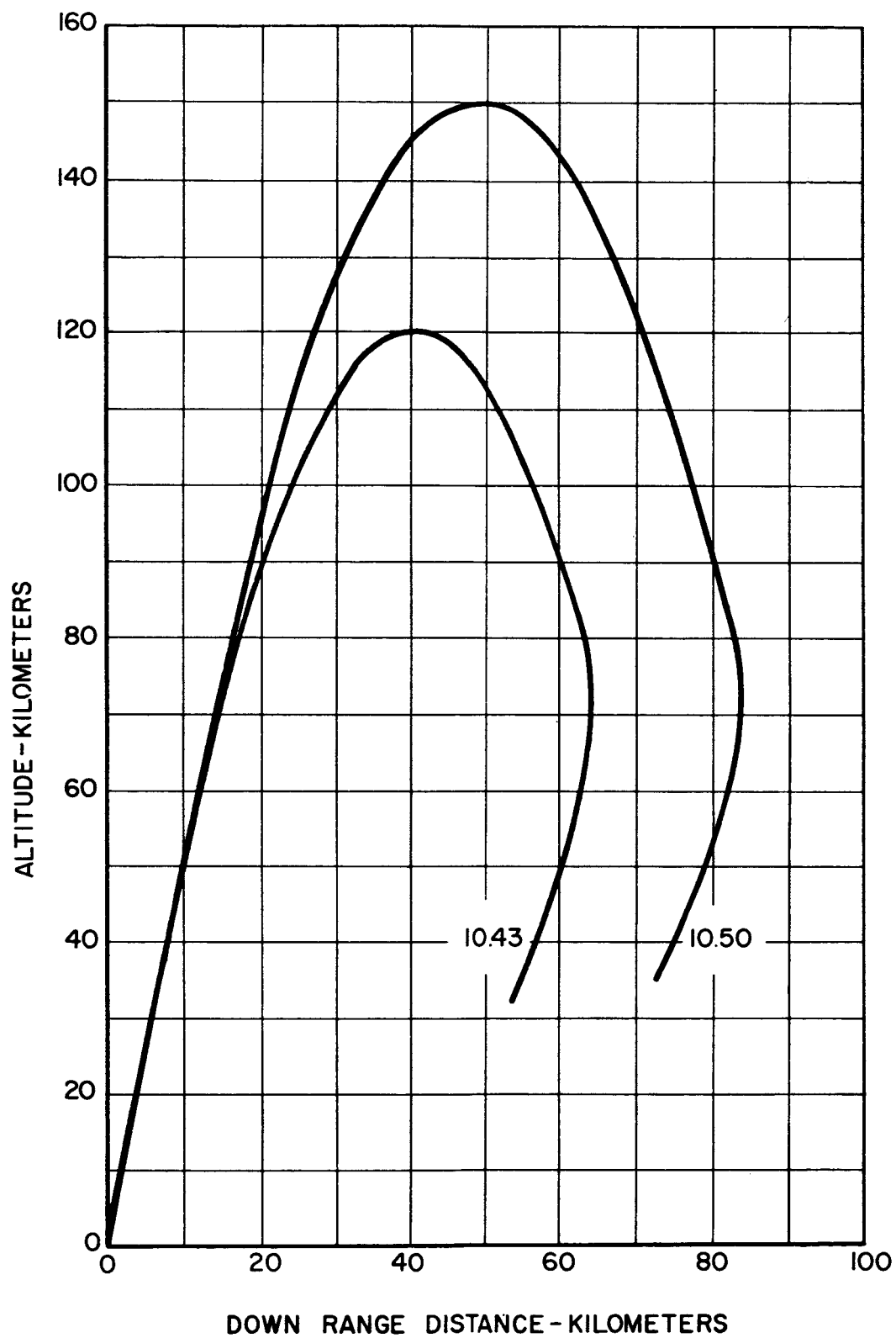


Fig. 4. Altitude vs. distance down range.

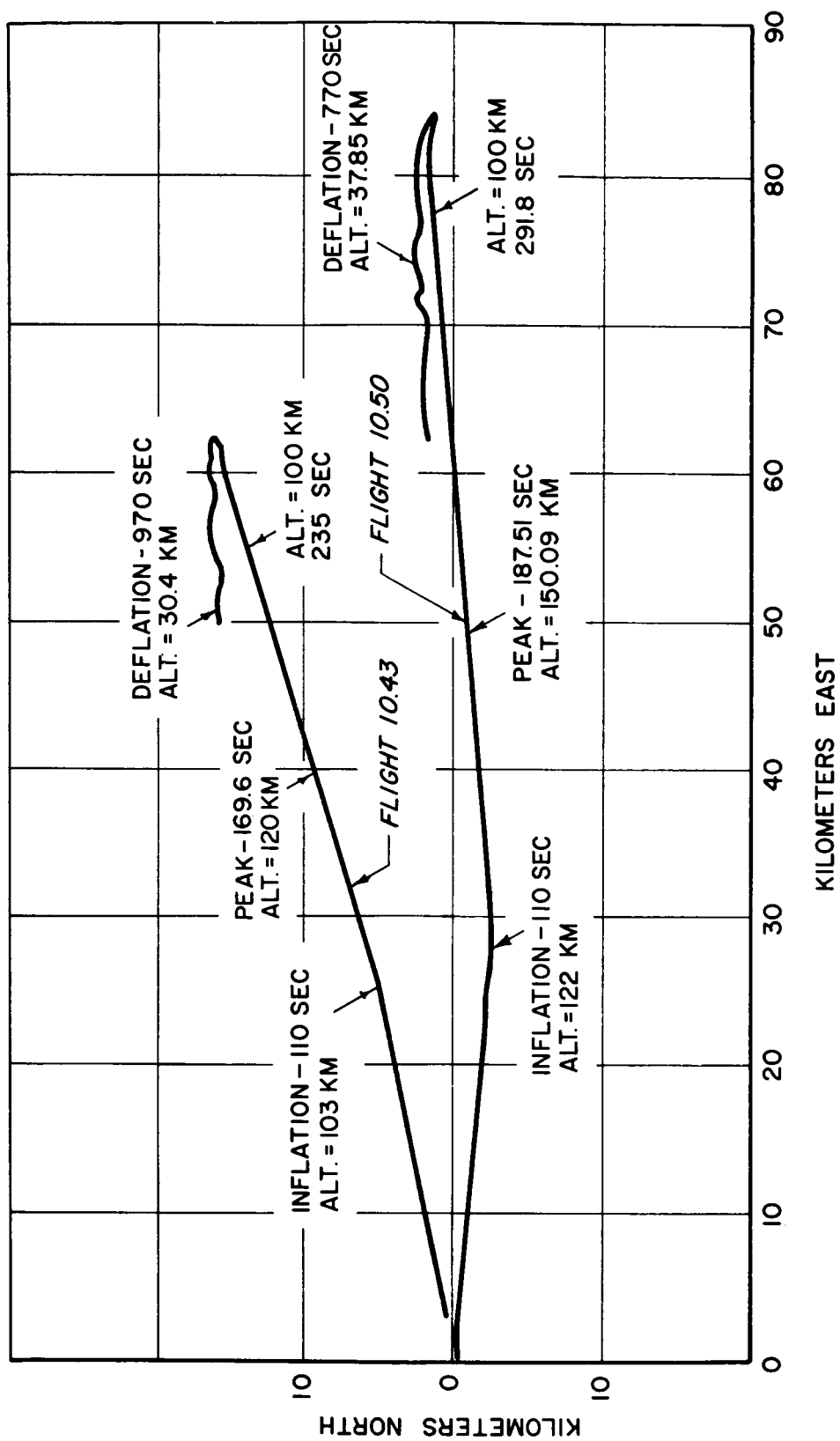


Fig. 5. Horizontal trajectory coordinates.

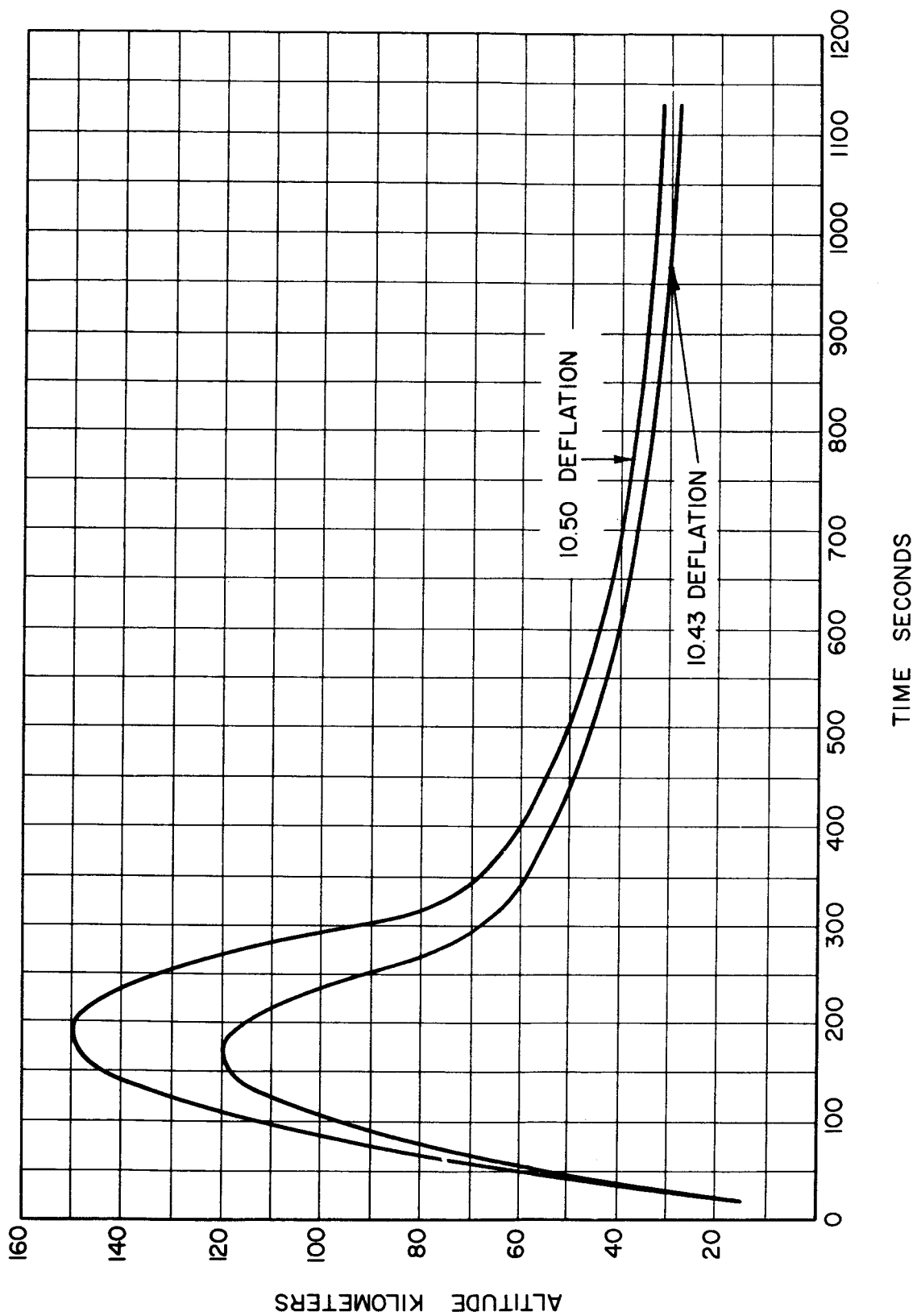


Fig. 6. Altitude vs. time.

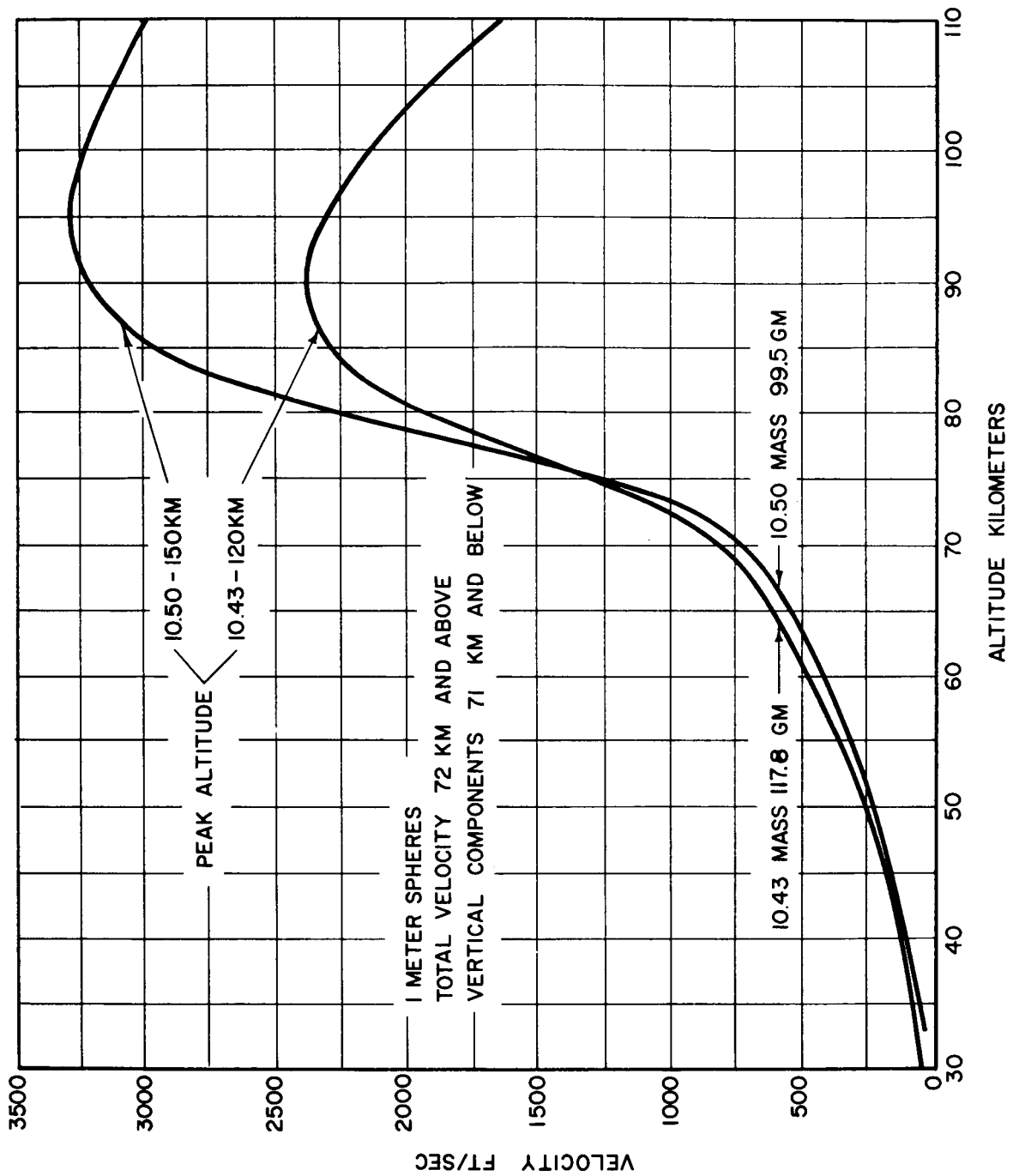


Fig. 7. Velocity vs. altitude.

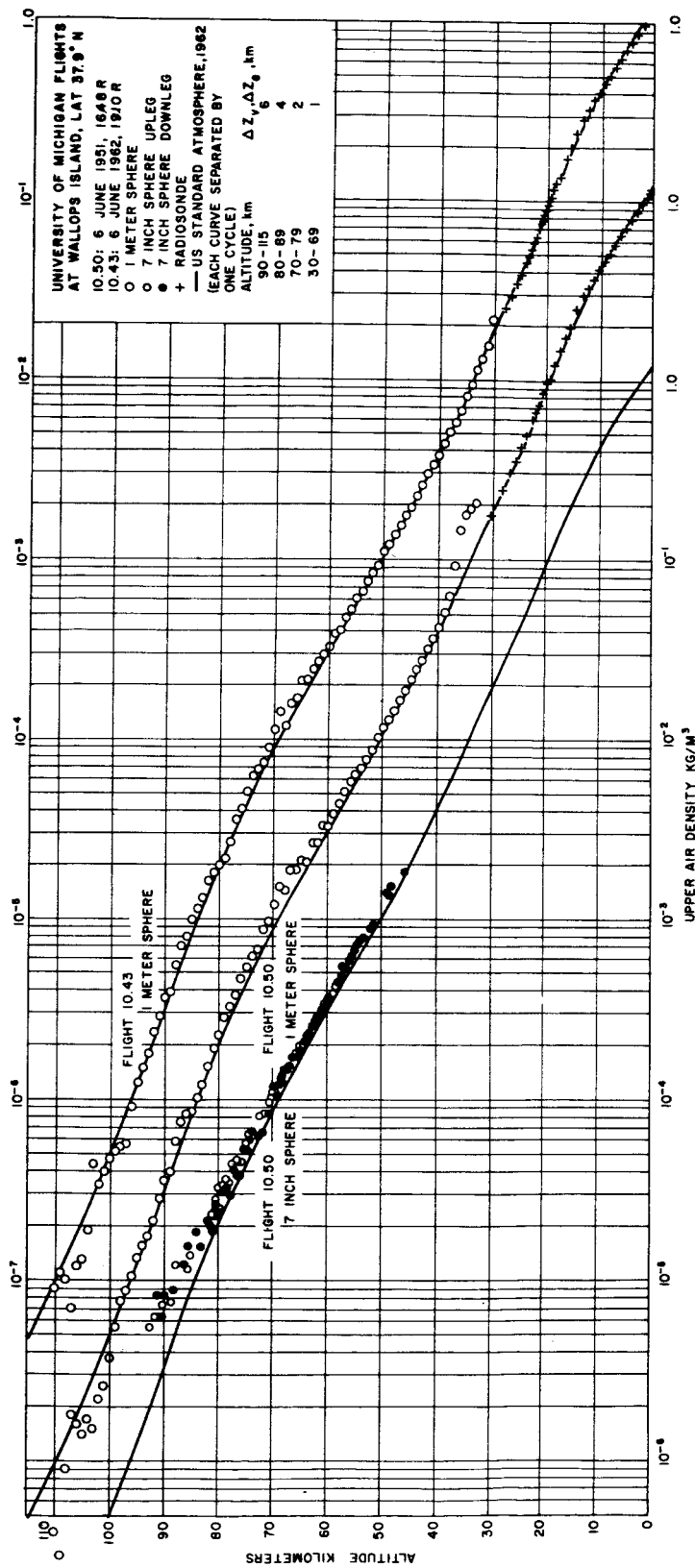


Fig. 8. Density profiles, Flights 10.50 and 10.43

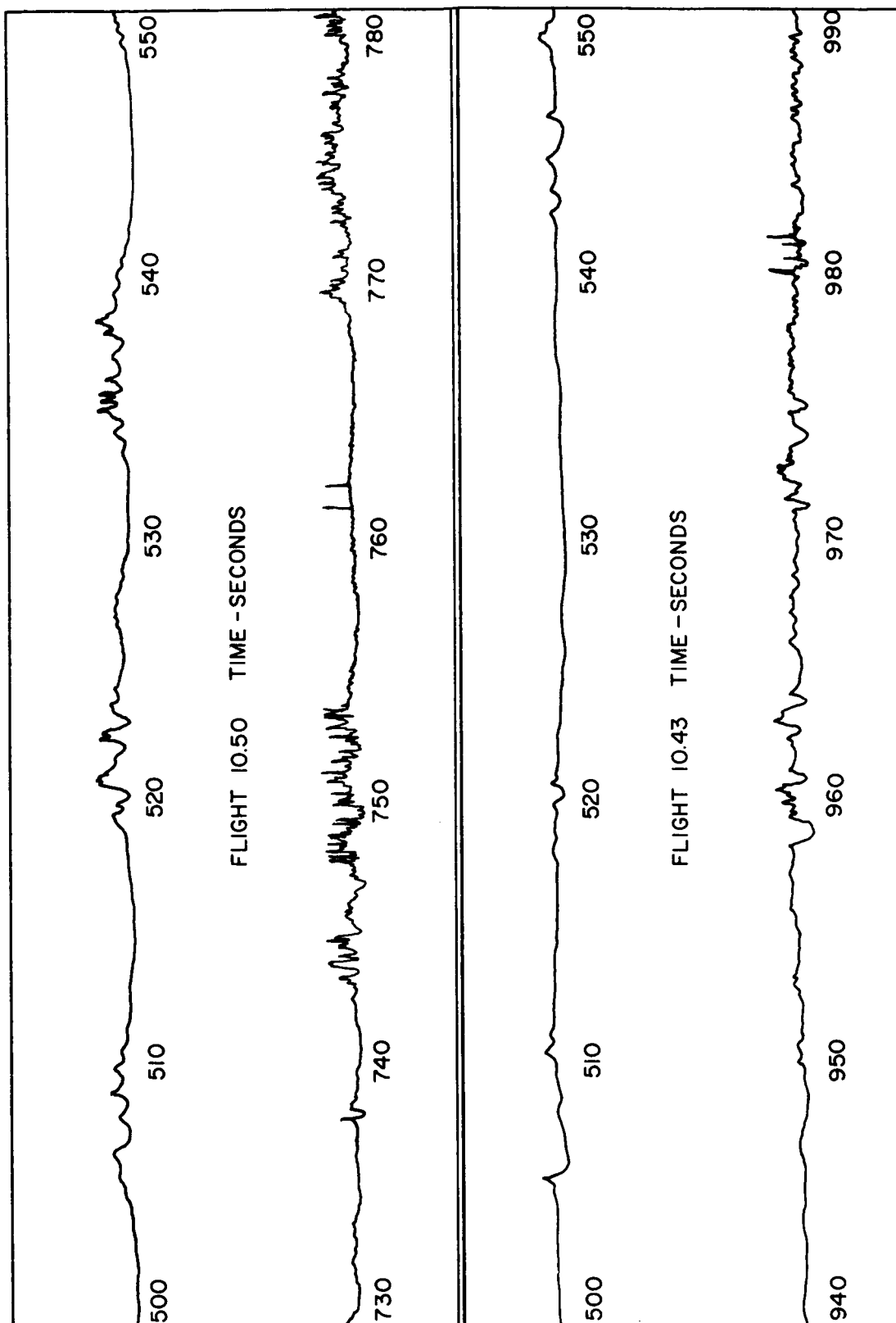


Fig. 9. FPS-16 radar AGC voltage.

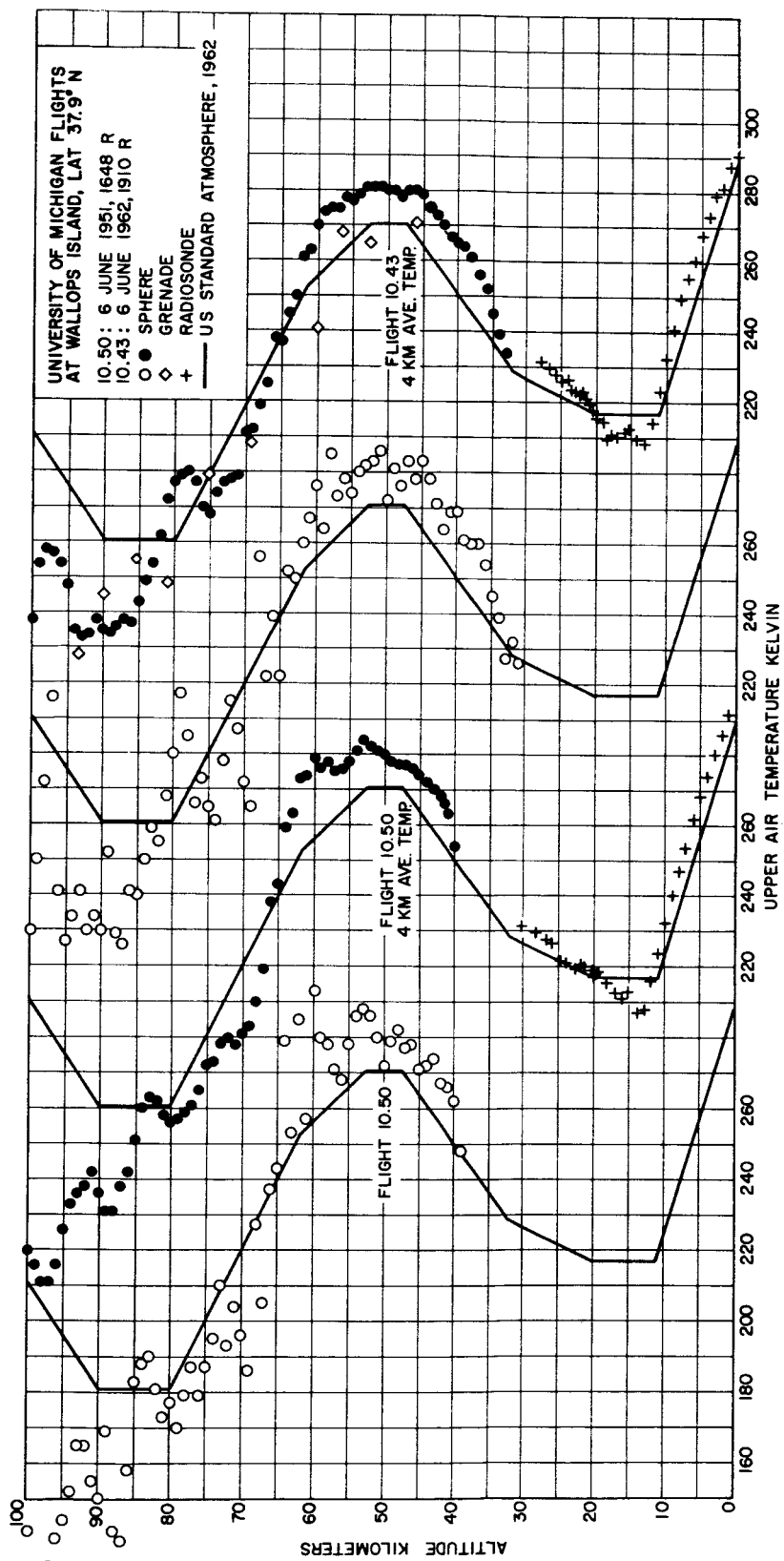


Fig. 10. Temperature profiles, Flights 10.50 and 10.43.

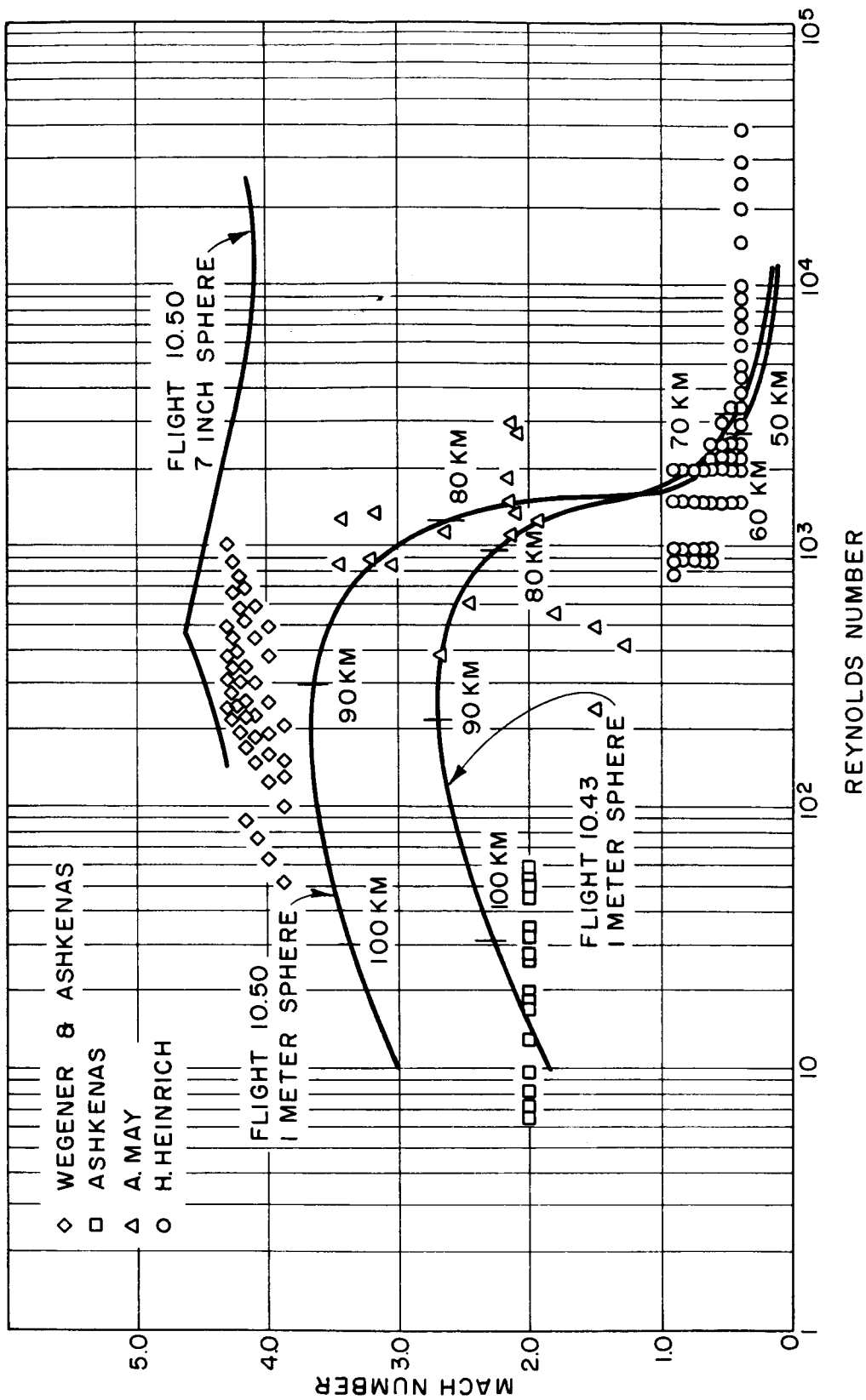


Fig. 11. Mach Number vs. Reynolds Number of falling spheres.

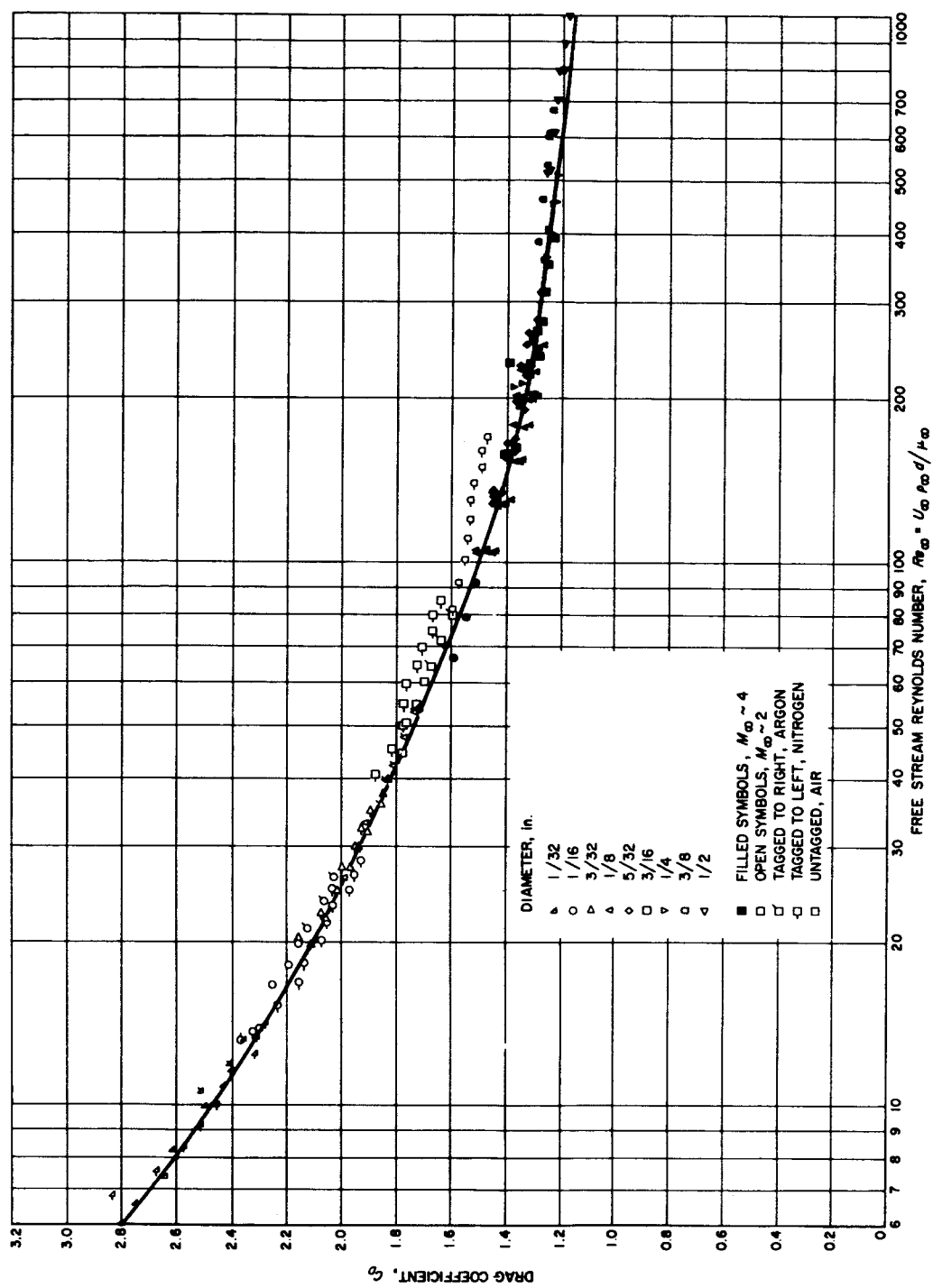
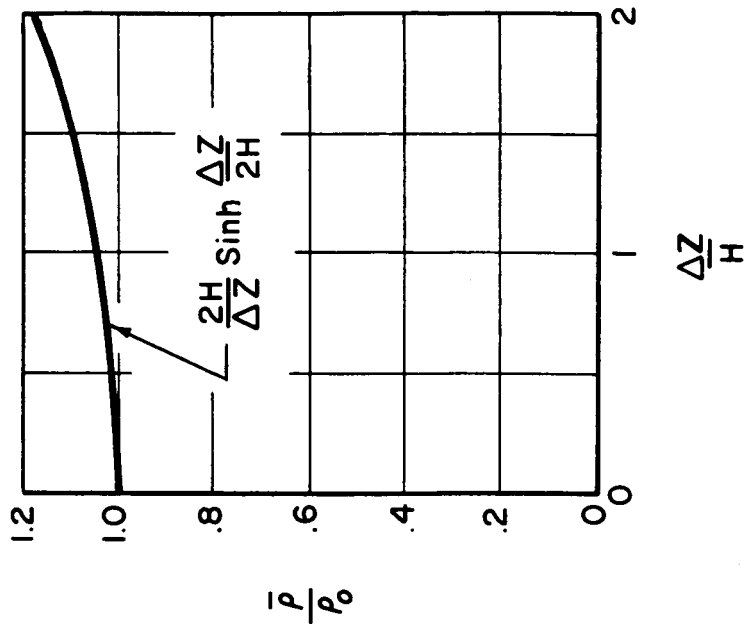
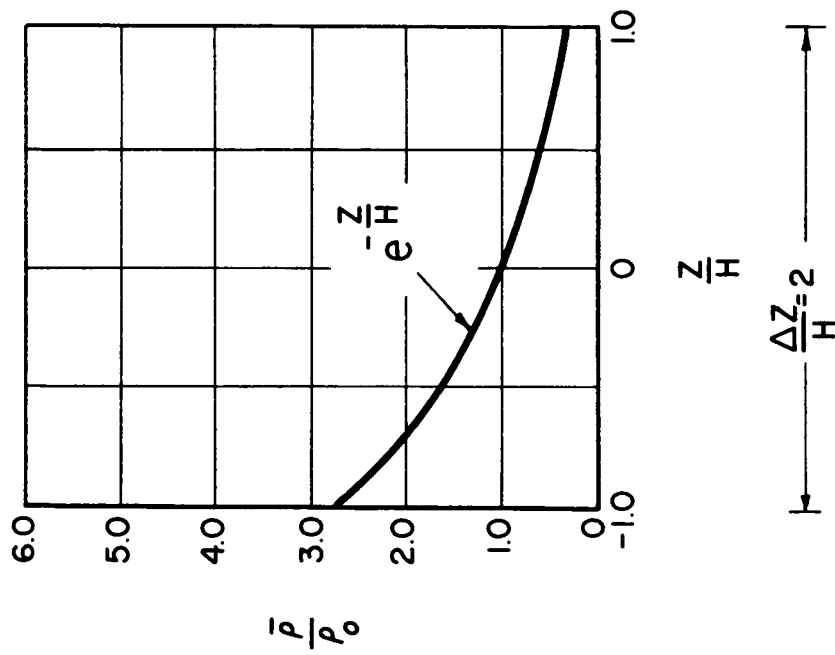


Fig. 12. JPL drag coefficient data. (From JPL Research Summary No. 36-12.)



$\rho$  MEAN DENSITY OVER INTERVAL  $\Delta z$   
 $\rho_0$  DENSITY AT CENTER OF INTERVAL  
 $H$  SCALE HEIGHT

Fig. 13.  $\bar{\rho}/\rho_0$  vs.  $L/H$ .

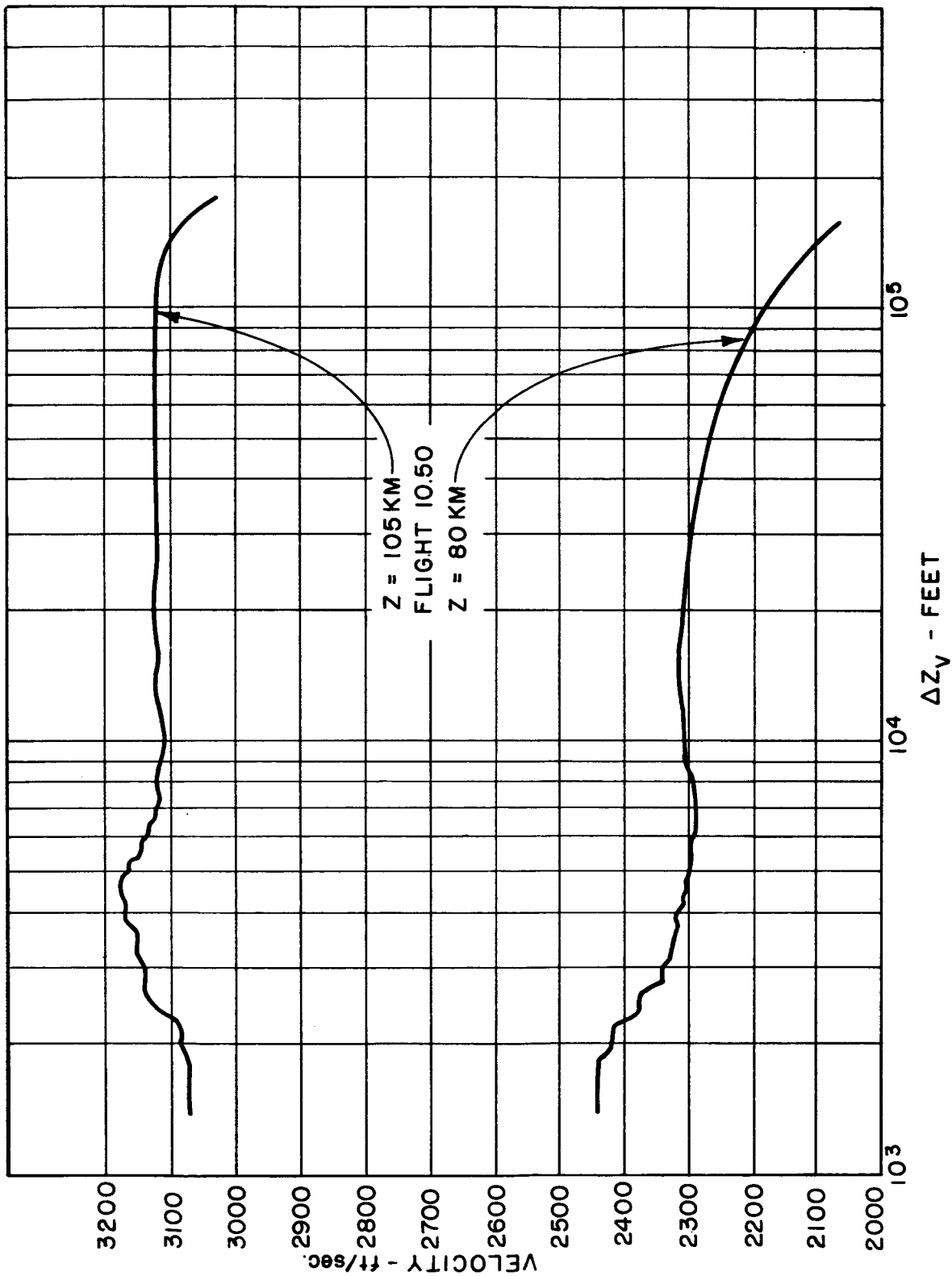


Fig. 14. Velocity vs. smoothing parameter  $\Delta Z_V$ .

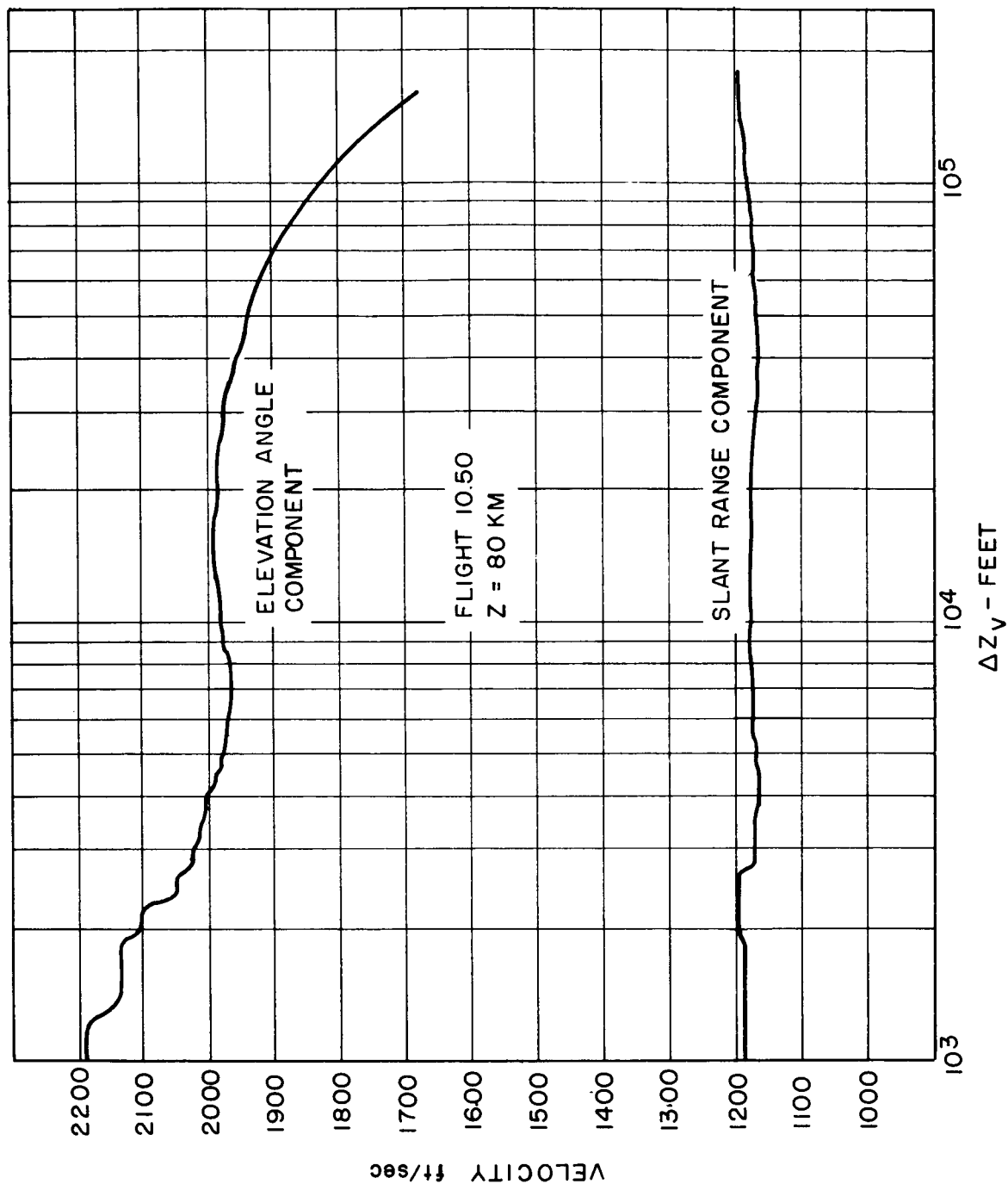


Fig. 15. Velocity components vs. smoothing parameter  $\Delta z_v$ , 80 km.

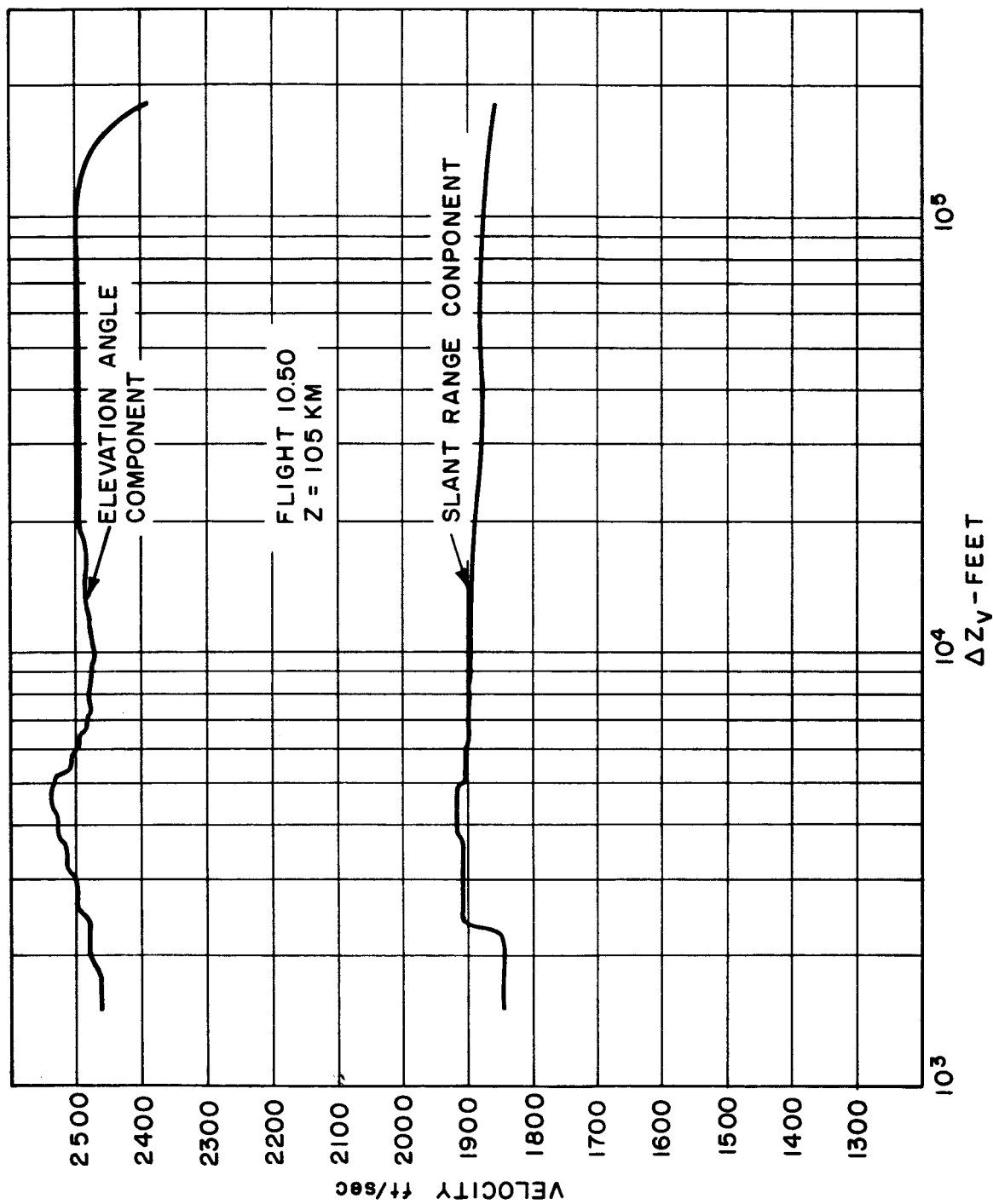


Fig. 16. Velocity components vs. smoothing parameter  $\Delta z_v$ , 105 km.

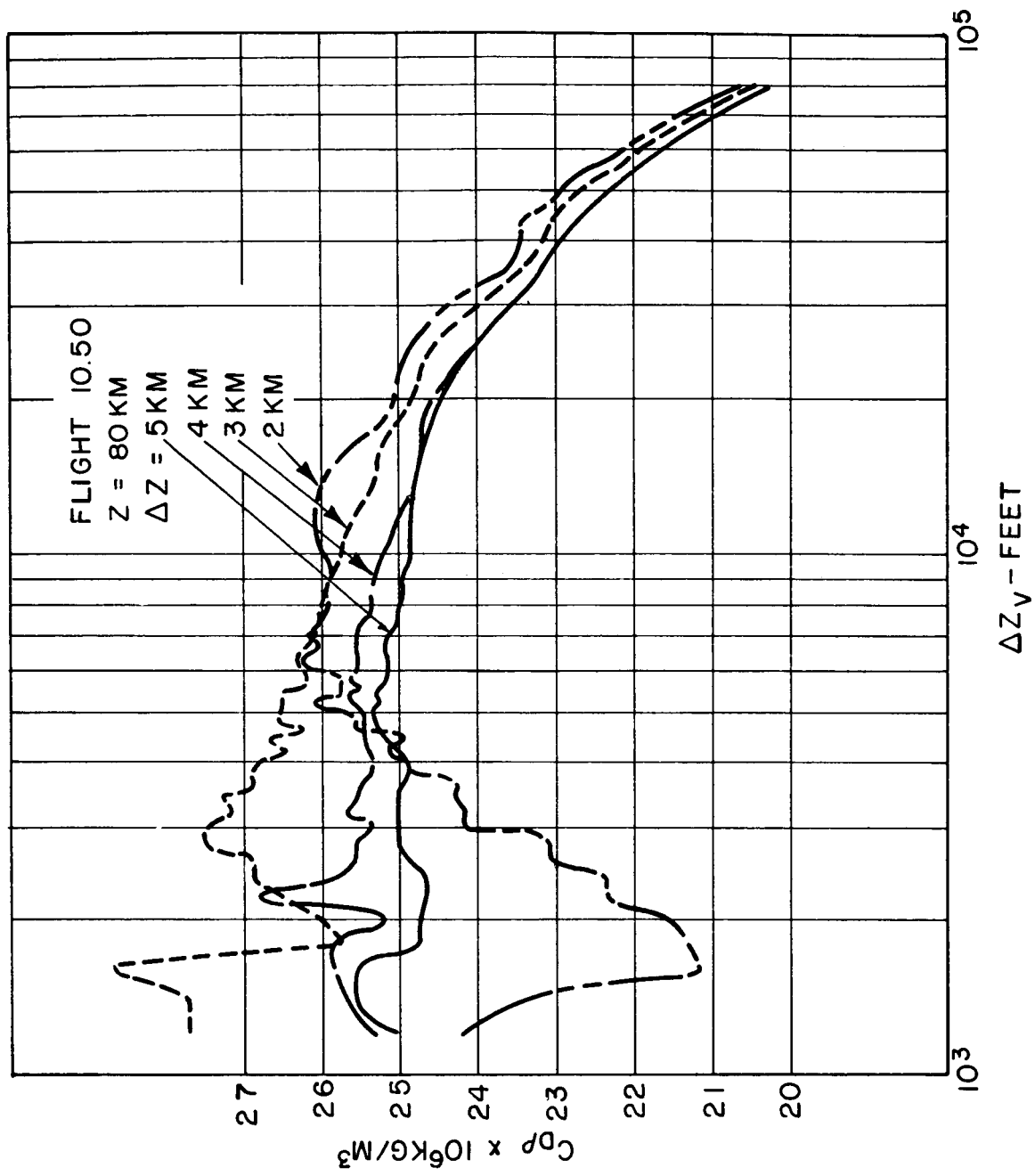


Fig. 17. Density function vs. smoothing parameter  $\Delta z_v$ , 80 km.

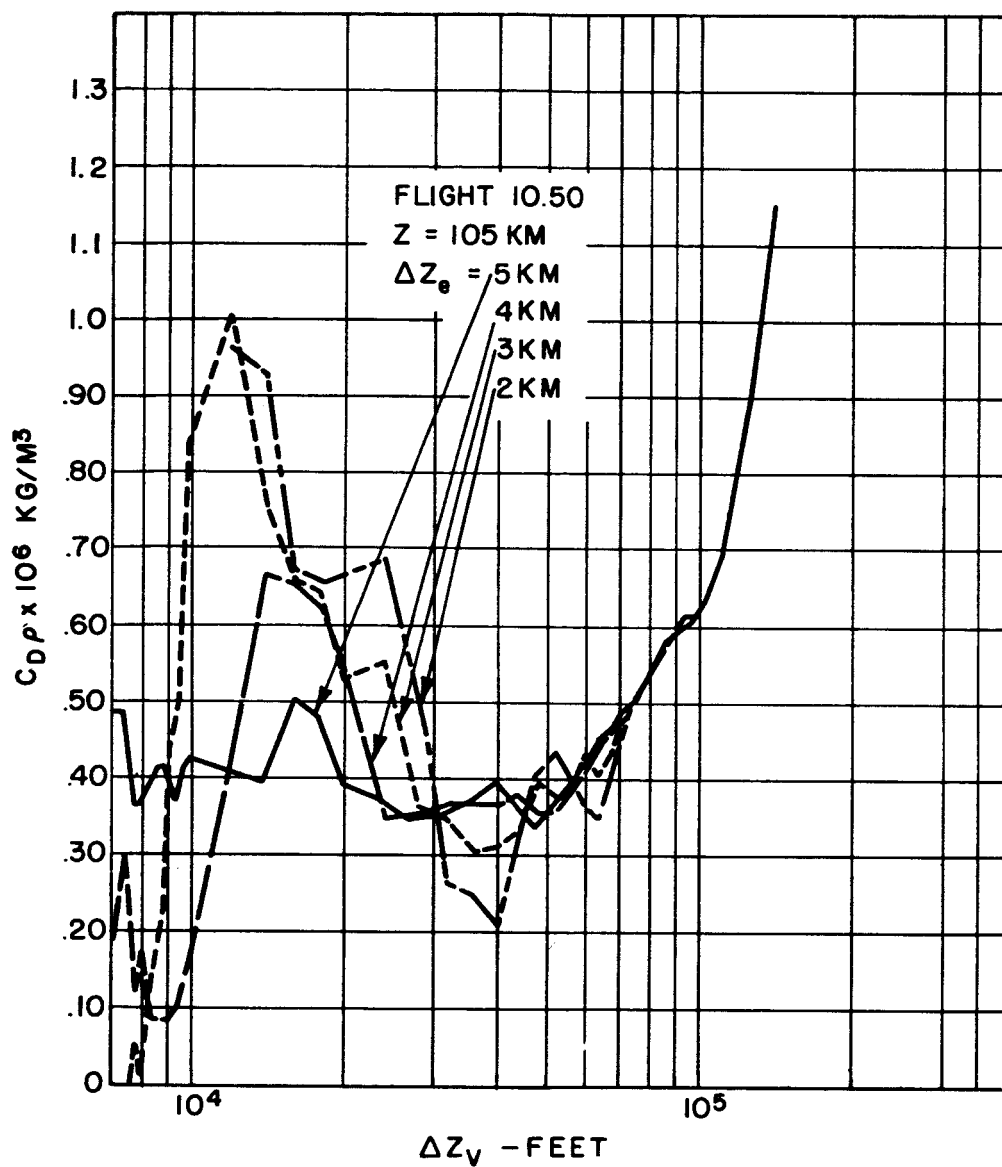


Fig. 18. Density function vs. smoothing parameter  $\Delta z_v$ , 105 km.